Universitat de Girona
Escola Politècnica Superior

Incoming Exchange Student - Master Thesis

Erasmus

Title of master course: Industrial Engineering

Title of master thesis: Experimental study of ultra-high performance fibre-reinforced concrete bolted connections under fatigue loads.

Document: Master Thesis

Student : An-Sophie De Meulenaere

EPS Advisor: Miquel Llorens
Department: Arquitectura i Enginyeria de la Construcció

Delivered on: 12/2015

Preface

To complete my education as a master student of science in industrial engineering construction, I had one last task to go, writing a master thesis. I made the choice to write my paper abroad. It has been a great experience that I could not have done without the support of some people.

First of all, I want to thank my parents. They gave me the opportunity to study for four years at the university. During my entire life, they have guided, encouraged and loved me. They were always there when necessary and helped me to become the person I am today. Because of them I could discover another country, another way of living, many different languages and most important of all, a lot of kind and interesting people.

Next I want to express my gratitude to my supervisor, Miquel Llorens, for giving me an interesting topic, for spending his valuable time on our meetings and for sharing his knowledge with me. I truly appreciate his guidance during the development of this thesis.

A last word of gratitude goes to my boyfriend and my friends at home for their love and support. I have neglected them a little the last couple of months but I hope that my hours on skype made up for it.

I wish you a pleasant reading .

An-Sophie De Meulenaere

Girona, 15 december 2015.

Abstract

Bolted unions especially designed for concrete are becoming a quite usual solution for connecting these elements to framed structures of any material. Its behaviour under fatigue loads -especially when the concrete member can be described as thin- must be carefully studied from a durability point of view. The objective is to assess these connections used in combination with ultra-high performance fibre-reinforced concrete under dynamic loads. In particular, the dynamic effects caused by the wind on these connections. The study consists of a theoretical and an experimental approach.

Experimental study of ultra-high performance fibre-reinforced concrete bolted connections under fatigue loads

De Meulenaere An-Sophie

Promotor: Llorens Miquel

I. Introduction

The use of ultra-high performance fibre-reinforced concrete (UHPFRC) became more popular because of the increasing demand for slender structures. A study was made about UHPFRC slabs in combination with bolted connections for a building in Marseille.[1] In this report, the actual tensile strength and the bonding of the bolt to the concrete was evaluated.

This master thesis was developed because of a lack of information about fatigue failure in such joints. The aim is to investigate the impact of cyclic wind loads on bolted connections with UHPFRC.

II. Procedure

Wind can be separated in four components to determine the necessary parameters to simulate the wind forces: the mean wind velocity component, the ramp component, the gust and the turbulence component. Fatigue failure is induced by dynamic loads, therefore only the gust component and turbulence component should be taken into account.

A servo hydraulic testing machine was used to perform the fatigue test. The used procedure was amplitude controlled and measured the maximum forces applied on the connection to generate a predefined displacement for every wind cycle. The output of the test should be transformed in a graphic represented in figure 1. [2]

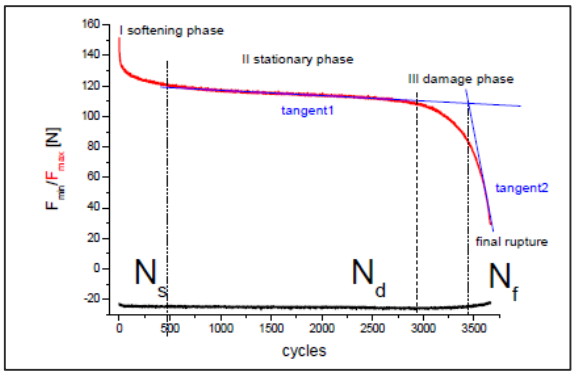

Figure 1: Different stage of fatigue failure

III. Results

A. *Experimental test*

The first 3500 cycles with an amplitude of 3,55mm did not have any worth mentioning effect. Therefore, amplitude was increased to 6,3mm for 700 cycles. The requiered amount of cycles applied on the connection with a controlled maximum displacement to induce fatigue failure, could not be determined anymore because of this change.

Instead, the weakest part of the connection was investigated. The amplitude was increased twice more to 9mm and 12mm for only 200 cycles. The maximum force was set out to the number of cycles applied on the test piece in figure 2.

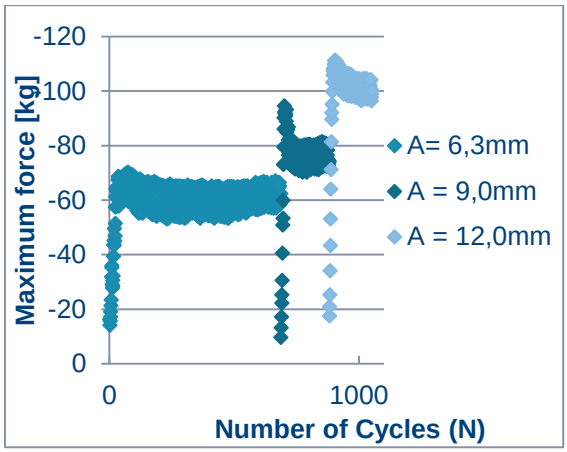

Figure 2: measured maximum force

The main observations of the test were the deformation of the metal plate to absorb the forces on the connection and the rotation of the slab to adjust itself to the applied forces, shown in figure3.

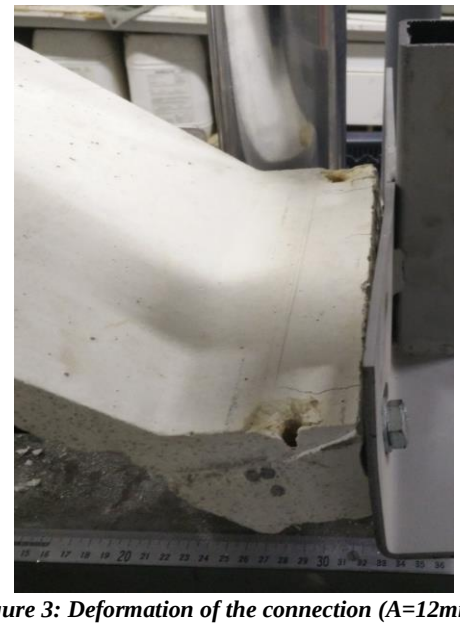

Figure 3: Deformation of the connection (A=12mm)

B. *Comparison with numerical model*

The bolted connection did not fail due to fatigue in the experimental test. Together with the change of amplitude of the gust, no value could be sustain in order to compare the test with an numerical model.

IV. CONCLUSION

The tests resulted in the deformation of the metal plate. This plate connects in reality the bolts and the concrete slab to a steel profile on the building. The bolts, the bonding to the concrete and the concrete itself did not receive any noticeably negative influences of the cyclic loads. The main conclusion of the tests was that the welds of the metal plate to the steel profile would probably be the weakest component of the connection. Further research should include studies about the various components of the connection and the different combinations of these elements.

Unfortunately, the tests did not result in a comparable value with a numerical model. A test with a longer duration and only one set of parameters should be excited to obtain such a value. To verify the result, the same experiment should be repeated several times.

ACKNOWLEDGEMENTS

A special thanks goes to my supervisor eng. M. Llorens for his expertise and guidance during this process. I truly appreciate his assistance and the sharing of his knowledge to develop this report.

This recognize that this research would not have been possible without the equipment of the Universitat de Girona. Therefore I would like to express my gratitude.

REFERENCES

[1] LLorens Miquel, Etude de brises soleil en beton fibre ultra haute performance, 2015.

[2] Major Z, Applicability of Displacement Controlled Fatigue Test Methods for Compliant Structures, 2012 .

Content

Preface **2**

Abstract **4**

Extend abstract **5**

Nomenclature **9**

Introduction **10**

1 State of the art **11**

1.1 Introduction *11*
1.2 History *11*
1.2.1 Bridges 12
1.2.2 Civil and architectural examples 12
1.3 Materials *13*
1.3.1 Mixture 13
1.3.2 Properties 14
1.4 Aim *15*
1.5 Conclusion *15*

2 Bolted connections **16**

2.1 Failure modes *16*
2.1.1 Tension strength failure 16
2.1.2 Shear failure mode 16
2.1.3 Net section tension failure mode 17
2.1.4 Bearing failure mode 17
2.1.5 Pull out failure 18
2.1.6 Fatigue failure 18
2.2 Types of connections *18*
2.3 Comparison *18*
2.3.1 Anchor length and strength 19
2.3.2 Structural strength 19
2.3.3 Binding to the concrete 20
2.4 Fixing socket with bolt *21*
2.4.1 Fixing Socket Pfeifer 21
2.4.2 Bolt hole 22
2.4.3 Tensile strength 22
2.5 Conclusion *22*

3 Wind **23**

3.1 Characterization *23*
3.1.1 Development 23
3.1.2 Variation in velocity 23
3.1.3 Estimation mean velocity 24
3.2 Test conditions *25*
3.2.1 Wind forces 25
3.2.2 Gusts 39
3.3 Conclusion *44*

4 Test in laboratory conditions **45**

4.1 History of wind performance evaluation *45*

4.1.1 FM 4470 and UL 580 standard 45
4.1.2 European and Norwegian load sequences 45
4.1.3 Wind tunnel 46
4.2 Fatigue 46
4.2.1 S-N curve 46
4.2.2 Cyclic stress 47
4.3 Design of the setup and procedure 47
4.3.1 First approach 47
4.3.2 Conclusion of first approach 49
4.3.3 Second approach 49
4.4 Experimental results 50
4.5 Conclusion 52

5 Theoretical approach 53

5.1 ANSYS procedure 53
5.1.1 Fatigue tool 53
5.1.2 Further process 54
5.2 Conclusion 54

6 Further research 55

General conclusion 56

References 57

Nomenclature

A_{fr}	Area swept by the wind
A_{ref}	Reference area
B^2	Background response factor, allowing for the lack of full correlation of the pressure on the structure surface
c_d	Dynamic factor
c_{dir}	Directional factor
$c_e(z)$	Exposure factor
c_f	Force coefficient
$c_{f,o}$	Force coefficient of structures or structural elements without free-end flow
c_{fr}	Friction coefficient
c_p	Pressure coefficient
c_r	Roughness factor
c_o	Orography factor
c_s	Size factor
$c_s c_d$	Structural factor
c_{season}	Seasonal factor
d	Depth of the structure (the length of the surface parallel to the wind direction)
F_{fr}	Resultant friction force
f_L	Non dimensional frequency
F_w	Resultant wind force
I_v	Turbulence intensity
k	Equivalent roughness
k_p	Peak factor
k_r	Terrain factor
L	Turbulent length scale
n_i	Natural frequency of the structure of the mode i
$n_{1,x}$	Fundamental frequency of along wind vibration
q_b	Reference mean (basic) velocity pressure
q_p	Peak velocity pressure
R^2	Resonant response factor, allowing for turbulence in resonance with the vibration mode
R_h, R_b	Aerodynamic admittance functions
S_L	Non dimensional power spectral density function
v_b	Basic wind velocity
$v_{b,0}$	Fundamental value of the basic wind velocity
v_m	Mean wind velocity
W	Wind pressure
Z	Height above ground
z_0	Roughness length
z_e, z_i	Reference height for external wind action, internal pressure
z_{max}	Maximum height
z_{min}	Minimum height
z_s	Reference height for determining the structural factor
Δ	Logarithmic decrement of damping
δa	Aerodynamic logarithmic decrement of damping
δd	Logarithmic decrement of damping due to special devices
δs	Structural logarithmic decrement of damping
η	Variable
ϕ	Solidity ratio, blockage of canopy
λ	Slenderness ratio
v	Up-crossing frequency
P	Air density
Σv	Standard deviation of the turbulence
Ψr	Reduction factor of force coefficient for square sections with rounded corners
Ψλ	Reduction factor of force coefficient for structural elements with end-effects

Introduction

Fatigue life became a very common topic the last couple of decades. This forms, together with a rising interest for ultra-high performance fibre-reinforced concrete (UHPFRC), a perfect combination for a new study. A lot of research has been done surrounding bolted connections, especially in combination with roof claddings. Nonetheless, there is a lack of information about fatigue life of bolted connections for ultra-high performance fibre-reinforced concrete.

UHPFRC slabs were used as wall claddings for a building in Marseille. They were attached to the main frame by bolted connections. Before the construction, different tests were performed to determine the tensile and compressive strength. The behaviour of the bolt in this type of concrete was investigated as well. These tests and results are described in a study made by M. Llorens (2015).

The aim of this report is to develop an experimental fatigue test for this bolted connection and to compare it with a numerical model. Generally, a wind tunnel test would be used to perform such kind of tests. Most universities and companies are not in the possession of this device because of the high purchase costs and the required space. Therefore a procedure should be developed to perform a fatigue test with a servo hydraulic machine.

In chapter one the state of the art of ultra-high performance fibre- reinforced concrete is summarized, followed by information about the mixture and properties of the concrete itself. The last topic of this chapter is a detailed description of the purpose of the concrete. The second chapter entails a comparison between different types of bolts together with previous tests performed on the concrete slab and the connection. The third chapter focusses on the simulation of the wind. In this chapter the necessary parameters for the experimental test, described in chapter four, are determined. This test was simulated according to the methods designed by Z. Major (2013). A theoretical approach to simulate this problem in a numerical model is discussed in chapter five. Finally some possible further research is summarised.

1 State of the art

1.1 Introduction

An increasing demand for innovation and expansion of techniques and materials in the construction industry, led to the development of stronger and more sustainable concrete types. In the last couple of decades, research offered new insights which resulted in the design of high performance concrete (HPC). Later on, the discovery of fibre-reinforced concrete and the need for secure, indestructible and sustainable concrete structures, arose a new wave of inventions from which emerged ultra-high performance fibre-reinforced concrete (UHPFRC) along with other concrete mixes.

Ultra-high performance fibre-reinforced concrete consists of a combination of cement with a higher strength than conventional cement, and steel or synthetic fibres. Adding fibres has several beneficial effects:
.- Improve the structural strength and ductility
.- Reduce the steel reinforcement requirements
.- Enhance resistance to impact- and abrasion.
.- Improve freeze-thaw resistance
.- Reduce crack widths and control the widths tightly, thus increasing durability
.- Enhance fire resistance

Concretes are declared as ultra-high performance concretes (UHPC) when their mixtures have a higher compressive strength than strength class C100/115. The typical compressive strength and uniaxial tension of UHPFRC is 150-200MPa and 7-15MPa respectively. This means that it can be classified under the category of UHP concretes. This new hi-tech material is perfect for structures or elements that demand a higher tensile, high compressive strength, high energy absorption capacity and a small thickness. Therefore, ultra-high performance fibre-reinforced concrete will be used in the context of this thesis. A short overview of the history of UHPFRC is given in paragraph 1.2 along with some examples. The mixture and properties are examined in the paragraph 1.3. In order to better comprehend the purpose of the UHPFRC-slabs, the objective is discussed paragraph 1.4 .

1.2 History

In the sixties, the creation of a high performance concrete with a compressive strength up to 800 N/mm² within laboratory conditions was the state of the art. Since then, the idea of developing a usable HPC was born. This subject became very popular two decades ago when Lafarga and Bouygues, two French construction companies, cooperated to initiate a research program about ultra-high performance concretes. The development period includes, inter alia, testing of the characterisations and the production of prototypes. Ten years later, their research was finished and a new material was developed with a high compressive strength, enhanced flexural resistance and an improved ductile behaviour, known as DUCTAL.

When UHPC was used more frequently, the need for guidelines arose and in 2002, Setra, a French company specialised in infrastructures and transport engineering, produced the first guidelines with recommendations about the use of the concrete. (Batoz, 2009). These guidelines can be divided in three main parts.

The first part contains the recommendations for the mechanical characteristics that should be obtained. Also the procedures for placement of the product and inspection during and after the process are mentioned. The second part provides the guidelines for the addition of fibres, non-prestressed reinforcements and non-reinforced elements. The third part discusses every component that influences the durability of the concrete.

1.2.1 Bridges

UHPFRC is often used for the construction or renovation of pedestrian and road bridges. In 1997, the first completed prestressed pedestrian bridge in ultra-high performance concrete was built in Sherbrooke (Canada), illustrated in Figure 1.1. Since then, UHPFRC caught the worldwide attention of a lot of engineers, academics and many governmental departments. Especially the government of Germany, Japan, USA and France financed an extensive research program which resulted in the development of new infrastructures around the world. Examples of the use of UHPFRC in bridges are shown in Figure 1.1 to Figure 1.3.

Figure 1.2 represents the Bourg-Les-Valence bridges in France. This experimental bridge was the first completed road bridge in UHPFRC in the world. It was unique for a bridge to have a bridge deck made of the fibre-reinforced concrete and even the joints between the precast beams consisted of a mix of UHPFRC cast in place.

One year later, the Seonyo Sunyudo footbridge in Seoul (South Korea), better known as the bridge of peace, shown in Figure 1.3, was finished as well. It connects the Sunyudo island to the city. For the first time in history, a footbridge was built with such a large span, 120metres, in this type of concrete. The characteristics of the fibre-reinforced UHPC made it possible to construct a slender arch in the middle of the bridge with various thin sections. The arch itself consist six precast segments which were joined together by cast in place joints.

Figure 1.1 Sherbrooke bridge, Canada 1997

Figure 1.2 Bourg-Les-Valence bridge, France 2001

Figure 1.3 Seonyo Sunyudo footbridge, South-Korea 2002

1.2.2 Civil and architectural examples

UHPC was initially used for constructions in the security business such as vaults and protective defence constructions. Because of the outstanding characteristics of this concrete, the use of it became more popular in civil, structural and architectural applications as well.

One of the first structural renovation applications with UHPFRC is the restoration of the Cattenom nuclear power plant in France, shown in Figure 1.5. The work consisted of the renovation of the thermal exchange supporting structure of the cooling towers. The lightness and the durability when exposed to an aggressive environment with varying temperature cycles, made girders in UHPFRC the perfect match for the renovation. These beams were manufactured on site and had the ability to be constructed under normal weather conditions.

Figure 1.4 Tollgate canopy Viaduct-de-Millau, France 2004

UHPFRC was also used in the construction of the Viaduct-de-Millau, more precisely for the tollgate canopy which is situated about 4km before the viaduct. The canopy is 100m long and almost 28m wide resulting in a surface area of 2,800m². This helicoidally structure, shown in Figure 1.4, contains 53 precast elements reinforced by metal fibres. One central prestress ties the elements together over the length of the canopy. It was the first structure of this size made out of metal fibre-reinforced UHPC.

An architectural example is the Zonnestraal Folly, located in Amsterdam (Netherlands) and constructed in 2005. The sunshade structure, Figure 1.6, was designed to represent the progression in the concrete industry of the past century. The roof has a surface of 8m by 8m and is divided in four precast ultra-high performance fibre-reinforced concrete squares supported by four beams. The four segments are connected by bolted joints and have a thickness of 25mm.

A Last example of civil applications is the expansion of the Airport Haneda in Tokio. As visible on Figure 1.7, the airport expanded their territory on sea. This brought a lot of difficult issues that had to be solved by engineers. The main topics to be discussed were: the durability, strength and low maintenance costs. Because of the low permeability, light weight and salt resistance, UHPFRC was chosen above conventional concrete for the concrete area of 192 000 m². In 2010, this impressive structure was completed.

Figure 1.5 Cooling towers of Cattenom, France 1999

Figure 1.6 Zonnestraal Folly, Netherlands 2005

Figure 1.7 Expansion Airport Haneda in Tokio, Japan 2010

1.3 Materials

1.3.1 Mixture

The most important ingredients of UHPFRC are cement, a significant volume of fibres, a low water/cement ratio, more micro-silica than in conventional concrete and the absence of aggregates bigger than 4mm. Table 1.1 contains the mixture of the ultra-high performance fibre-reinforced concrete used for the experimental study in chapters 0 and 5.

Table 1.1 Mixture of UHPFRC

Material	Characteristics
Cement	White CEM I 52.5 R
Filler	Limestone filler
Admixtures	Super plasticizers (high range water reducer)
Water	Without any impurities or silt
Granulates	Aggregates up to 1.5mm
Micro-silica	Aluminosilicate pozzolan
Fibres	Resistant to alkaline (synthetic fibres)

Usually the fibres behave as a highly anisotropic material. When pouring the concrete, they are oriented in a disorderly way. But during the horizontal spread of the concrete in the precast mould, the fibres are given an orientation in the longitudinal direction along with the streamlines of the viscous flow. Because of the volumetric geometry and differences in thickness of the concrete slabs, it is impossible to control the fibre direction for the elements during the filling process. Therefore, the reaction of the fibres will not be the same as described in the previous case.

The slab is water and oil repellent because of a treatment based on an aqueous solution with a fluorinated acrylic copolymer. The humectant does not form a film on the concrete which gives the possibility for the threated substrate to evaporate.

Other advantages of the water repellent treatment:
.-The product is resistant to abrasion and UV.
.-It is invisible when it is dry. Thus it does not change the colour or external appearance of the concrete.
.-It modifies the surface tension of the substrate, preventing the penetration of water, air pollution, etc.
.-The appearance of efflorescence, mushrooms and lichens on the outer surface of the slab will be reduced.
.-It protects the UHPFR concrete against damage caused by frost.
.-The product is non-toxic, biodegradable and inflammable.

1.3.2 Properties

Three main influences on ultra-high performance fibre-reinforced concrete determine most of the characteristics: fibres, a low water-cement ratio and a high micro-silica ratio.

Fibres reduce the initial requirements of conventional reinforcement for concrete. They increase the tensile, shear and bending tension strength which leads to an improvement of the ductility. The deformation behaviour changes as well. Fibres also cause and increase of resistance to impact- and abrasion, fire resistance and freeze-thaw resistance.

The second major influence on concrete is the water-cement ratio. This is the amount of water compared to the amount of cement used in the concrete mix. The w/c-ratio used in UHPFRC is very low, around 0.20 or 0.25, to reduce the fraction of the capillary pores and to gain a higher strength and durability. The viscosity increases as well, therefore, plasticizers or super-plasticizers are needed to adjust the workability because otherwise the concrete mix would become too dense to use.

Micro-silica, also known as a supplementary cementitious material, is used to obtain a bigger compressive strength and higher brittleness than conventional concrete. By adding micro-silica, the pores between the cement parts are filled with this compound and resulting in a better packing density. The smaller pores lead to a reduced permeability of the concrete and a better protection for the UHPFRC against sulphates and chlorides.

Summarized improvement of properties of UHPFRC:
.- Improvement of the structural strength (tensile, shear and bending tension) and stiffness.
.- Reduction of the steel reinforcement requirements due to the steel fibres.
.- Enhanced resistance to impact, fire and abrasion.
.- Reduced crack widths and control the widths tightly, thus increased durability.
.- Low permeability which improves thermal resistance.
.- Need for plasticizers or super-plasticizers.
.- Cost-effective.
.- Low self-weight.
.- Could be used for very thin structures.

1.4 Aim

The assistance from concrete-engineers was invoked for the design of a new hospital in Marseille. As illustrated in Figure 1.8 and Figure 1.9, the façade elements were designed in concrete. The choice was made to use ultra-high performance fibre-reinforced concrete for the slabs due to the properties of the concrete. Because of the characteristics of the fibre reinforcements, as previously discussed, it was possible to design the slabs with a small thickness.

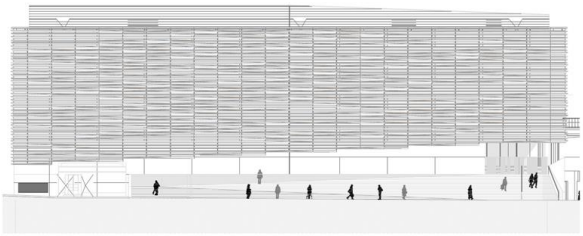

Figure 1.8 Design of the new hospital in Marseille

Figure 1.9 Completed realisation of the hospital in 2013

The façade elements, Figure 1.10, have a length of 2,85m and a minimum thickness of 9mm. They are connected to the building with bolted joints. Studies have been made about the characteristics of the slabs, the strains and deformation under various loads. (Llorens, 2015) Chapter 4 contains an experimental study to evaluate how certain connections will react over time under dynamic loads and in particular under wind loads.

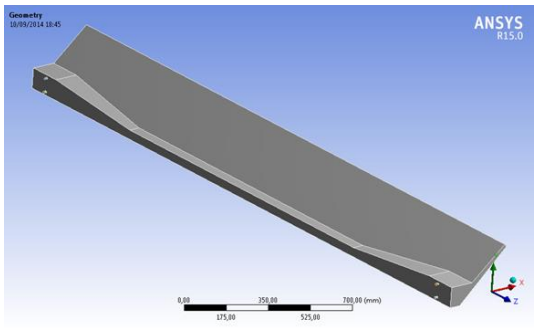

Figure 1.10 UHPFRC slab

1.5 Conclusion

The use of ultra-high performance fibre-reinforced concrete for structures is rapidly gaining more popularity due to the important improvements of properties. The thickness of structures or elements can be reduced because of the higher structural strength of the concrete. This creates a lot of new opportunities in terms of structural and architectural design. Within the scope of this thesis, thin concrete slabs of 2,85 meter will be used. However, UHPFRC is also adequate for the construction of high buildings, bridges, light-weighted structures etc.

2 Bolted connections

The connection between different elements is one of the most important aspects of structures and should be carefully designed. Failure of a connection could have an influence on many members of the construction. One of the main advantages by using mechanical bolted connections instead of cast in place mixtures, is the immediate strength of the connection. There is no curing time required, thus the construction time could be decreased causing a reduction of the installation costs. In this chapter various bolted connections will be discussed and compared in order to select the most suitable joint.

2.1 Failure modes

According to EN 1993-1-8 (2005), individual fasteners could be susceptible to failure if they are inadequate by one of the different resistance modes:
.- Due to tension strength failure
.- Due to shear resistance = Bolt shear failure mode
.- Due to bearing resistance = Bearing failure mode
Aside from the failures modes in EC 3 especially for the steel member, other ways of failure can occur.
.- Net section tension failure
.- Pull out (Tear out) failure
.- Fatigue failure

2.1.1 Tension strength failure

Bolts possess a certain tensile strength and are therefore divided in bolt classes.

Bolt class	4.6	4.8	5.6	5.8	6.8	8.8	10.9
f_{yb} (N/mm^2)	240	320	300	400	480	640	900
f_{ub} (N/mm^2)	400	400	500	500	600	800	1000

Figure 2.1 EC3, Nominal values of the yield strength fyb and the ultimate tensile strength f_{ub} for bolts

Bolts must not exceed the tension resistance:

$$F_{t,Rd} = \frac{k_2 \, f_{ub} \, A_s}{\gamma_{M2}}$$

With: f_{ub}: Ultimate tensile strength
A_S: Tensile stress area of the bolt
γ_{M2}: Partial safety factor for joints
k_2: Stiffness coefficient

Figure 2.2 EC3, Tension resistance

2.1.2 Shear failure mode

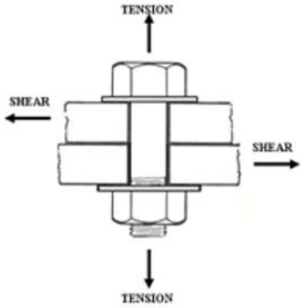

Figure 2.3 Shear

As the name of the failure mode already gives it away, this mode is related with shear strength. Shear stresses are generated by perpendicular loads acting on the bolts. The resistance of the bolts against shear depends on the bolt grades. The shearing of bolts may occur in two different parts of the bolts. In the threaded part of the bolt which is the area at the root of the bolt, and in the unthreaded part of the bolt, alias the upper part of the bolt. A and α_v are determined by through which part the shear plane passes.

The shear resistance not to be exceeded is:

$$F_{v,Rd} = \frac{\alpha_v \ f_{ub} \ A}{\gamma_{M2}}$$

- where the shear plane passes through the threaded portion of the bolt (A is the tensile stress area of the bolt A_s):
  - for classes 4.6, 5.6 and 8.8:
    $\alpha_v = 0,6$
  - for classes 4.8, 5.8, 6.8 and 10.9:
    $\alpha_v = 0,5$
- where the shear plane passes through the unthreaded portion of the bolt (A is the gross cross section of the bolt): $\alpha_v = 0,6$

With Fv,Rd: Shear resistance
α_v: Correction factor (threaded)
f_{ub}: Ultimate tensile strength
A: Tensile stress area of the bolt (threaded)
A: gross cross-section of the bolt (unthreaded)
γ_{M2}: Partial safety factor for joints

Figure 2.4 EC3, Shear resistance

2.1.3 Net section tension failure mode

Thin plates are especially sensitive to net section failure. When holes are drilled in the concrete, discontinuities are caused in the geometry of the plates. This causes higher stress concentrations in the areas close to the holes. The stresses could initiate necking of the bolt, which results in a rupture of the bolt. It depends of the tensile strength and the ductility of the concrete if the bolt cracks immediately (brittle failure) or not.

2.1.4 Bearing failure mode

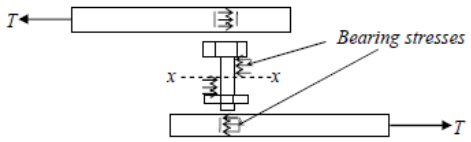

Bearing failure will occur to individual bolts due to compressive strength on the bolt. This is induced by a high stress concentration on the steel bolt.

Figure 2.5 Bearing stresses

The bearing resistance not to be exceeded is:

$$F_{b,Rd} = \frac{k_1 \, a_b \, f_u \, d \, t}{\gamma_{M2}}$$

where α_b is the smallest of α_d ; $\frac{f_{ub}}{f_u}$ or 1,0;
in the direction of load transfer:

- for end bolts: $\alpha_d = \frac{e_1}{3d_0}$; for inner bolts: $\alpha_d = \frac{p_1}{3d_0} - \frac{1}{4}$

perpendicular to the direction of load transfer:

- for edge bolts: k_1 is the smallest of $2,8\frac{e_2}{d_0} - 1,7$ or 2,5
- for inner bolts: k_1 is the smallest of $1,4\frac{p_2}{d_0} - 1,7$ or 2,5

With

Fb,Rd: The design bearing resistance per bolt.
α_b: Correction factor
f_{ub}: Ultimate tensile strength
f_u: Nominal tensile strength
d: Nominal bolt diameter
t: Plate thickness
γ_{M2}: Partial safety factor for joints
k_1: Stiffness coefficient

Figure 2.6 EC3, Bearing resistance

2.1.5 Pull out failure

Pull-out failure is related to the bonding between the bolts and the concrete, and to the material tensile strength. In this failure mode, the fastener is pulled out of the concrete because the concrete was not able to develop strength high enough to resist tensile forces on the bolt. In other words, the bonding to the concrete is not sufficient enough. Related to this failure mode is end-pull out failure. If the distance from the end of the concrete and the centre of the bolt is less the three times the diameter of the bolt, the bolt could be pulled out as well.

2.1.6 Fatigue failure

Materials exposed to dynamic/cyclic loads such as wind could rupture before one of the previous failure modes can occur. This type of failure is known as fatigue failure. Fatigue is a progressive process where damage increases by fluctuating stresses. It is initiated by small micro-cracks of the material caused by geometrical discontinuities which causes higher local stresses. The small cracks grow and coalescence until the cross-section is reduced to a remaining area of the bolt that cannot longer bear the loads which finally leads to rupture.

2.2 Types of connections

To determine a sustainable connection between ultra-high performance fibre-reinforced concrete slabs and a framed structure of any material, two main groups of fasteners can be distinguished based on the method of binding with the concrete: Chemical fasteners and mechanical fasteners.

Chemical anchors are fastened in the concrete by bonding the metal components to the inner surface of a predrilled hole with an adhesive or epoxy. These mortars need some time to cure, which is a significant disadvantage compared to the mechanical or expansion anchors. Once the adhesives or epoxies are hardened, they have gained their full strength and the fastener will be able to transmit the equal loads as the mechanical anchors depending on the type of bolt. The predrilled hole should be carefully cleaned because loose particles or dust can reduced the strength of the bonding. The quality of bonded connections must be strictly monitored since creep deformations can occur.

The second type of fasteners is the mechanical anchors. A broad variety of mechanical fasteners has been developed. Best known are screw anchors, bolts and nuts, undercut anchors and expansion fasteners. The latter type of fasteners is anchored to the concrete by expansion of the outer parts after inserting them in pre-drilled holes. Tensile forces can be transferred by friction and through the expanded parts. For most of the mechanical anchors, predrilled holes should be made and carefully cleaned out as well. Another solution is placing and positioning the bolts in the mould before the concrete is casted.

In view of the function of the ultra-high performance fibre-reinforced concrete slabs, both types of fasteners could be used. Therefore, in the next section, some chemical and mechanical anchors shall be analysed and compared in order to select the best type of connection in the purpose of the slabs.

2.3 Comparison

In order to select which connection is most suitable, three main features should be analysed:
.- Structural behaviour of the connection under bending and shear.
.- The quality of the binding system to the surrounding concrete.
.- Length of the bolts to make it possible to place it within the available limited space (less than 70 mm)

The following paragraphs contain a comparison of these characteristics of the bolts, based on technical files from Confast, Hilti, Construction fixings, Pfeifer and Halfen. Not all the characteristics were given by the supplier. Therefore some spaces were marked with a '/'. As first, the anchor length will be taken into account. Followed by the structural strength (tensile, shear and bending resistance), to finish with comparison of the bolts based on the quality of the binding system.

2.3.1 Anchor length and strength

The anchor length of the bolt, is the length needed in the concrete to secure the anchor. In most cases, two different lengths are given in technical data files, the length of the bolt and the minimum length that the bolt has to be inserted. This latter is called the anchor length.

In this case, the maximum anchor length allowed is 70mm because of the shape of the concrete slab. For each type of connection, there exist various bolts with different lengths and strengths.
If more than one bolt of a certain type occurs to be sufficient, the choice has been made to compare those with the biggest length less than 70mm, in combination with the highest tension and shear resistance. Thirteen different types of connections are compared in Table 2.1.

Table 2.1 Comparison Anchor length

Brand	Sort of bolt	Type	Chemical or Mechanical	Anchor length [mm]	Sufficient
Confast Hilti	Concrete lag shield anchor	¾'' Short	Mechanical	51	X
	Screw anchor	HUS3-H8	Mechanical	< 70	X
	Concrete wedge anchor	HSA M8	Mechanical	54	X
	Heavy duty expansion anchor	HSL-3 M8	Mechanical	80	
	Anchor rod + injective mortar	HIT-Z M8x80 HIT-HY 200-A	Chemical	80	
	Anchor rod + injective mortar	HIT-V-5.8 M8x80 HIT-RE 500	Chemical	80	
	Sleeve anchor	HLC M8	Mechanical	50	X
	Undercut anchor	HDA-TR RVS M10	Mechanical	>100	
Constr. Fixings Pfeifer Halfen	Recison anchor stud steel + solvent free pure epoxy	Gr5.8 ZYP	Chemical	80	
	Fixing socket with bolt	No 05.000.183	Mechanical	65	X
	Drop in anchor + screw 8.8	HB -E M 12	Mechanical	50	X
	High load anchor	HB-SZ-S 10-0 M6	Mechanical	67	X
	Anchor stud + 2-component adhesive, Styrene free	HB-VMZ-A 40 M8-15/65 GV	Chemical	65	X

2.3.2 Structural strength

Another subdivision can be made of the use of the anchorage system and the magnitude of the loads it can manage. It should be mentioned that the tensile- and shear strength is bigger in non-cracked concrete than in cracked concrete. In Table 2.2 (Comparison quality bolted connections with tension, shear en bending resistance) it is assumed that the ultra-high performance concrete is non-cracked.

The data was provided by the different suppliers. Each has its own manner of presenting the necessary information. The characteristic tensile and shear resistance was the most evident to compare for the various technical files.

Table 2.2 Comparison quality bolted connections with tension, shear en bending resistance

Type	Specifications	Tensile [kN]	Shear [kN]	Bending [Nm]	Useful
Lag shield anchor	-Has to be used with a lag bolt -Light to medium duty in concrete	10,43	11,92	60	X
Screw anchor	-Reusable -Sufficient for high loads	9,0	12,8	46	X
Wedge anchor	-Only in non-cracked concrete -Medium to heavy duty	16,5	10,6	21,7	X
Heavy duty expansion anchor	-Only exposed to indoor conditions -Heavy duty	23,4	31,1	30	
Anchor rod HIT-Z	-Usable in external conditions - Medium to heavy duty	24	12	24	X
Anchor rod HIT-V	-High loading capacity -High corrosion resistant	18	9	10	X
Sleeve anchor	-Various head shapes -Light duty in concrete	2,1	3,2	5	
Undercut anchor	-Indoor, dry conditions -Heavy duty in concrete	46	71	60	
Anchor stud + pure epoxy	-High chemical resistance -High performance	19	9,5	10,9	X
Socket with bolt	-Installation in the edge of structural elements -Installation in column shaped elements	16	8,0	/	X
Drop in anchor + screw 8.8	-To be used in dry room -Medium to heavy duty	11	12	60	
Highload anchor	-To be used in non-cracked concrete -Medium to heavy duty	7,6	10,1	6,9	X
Anchor stud + Styrene free	-Usable in external conditions - Medium to heavy duty	6,6	8	17,1	X

2.3.3 Binding to the concrete

All of these bolted connections are chosen for their capacity to be used in concrete but the quality of the binding system could differ significantly. Analysing the anchor length of the different types of bolts in Table 2.1, resulted in seven usable bolted connections. Six of the connections require too much space for anchorage. In Table 2.2, all thirteen fasteners are compared based on their structural strength and their usage. Only eight out of the thirteen connections could be called sufficient for the use in external environmental conditions.

In Table 2.3, a ranking is presented from the best suitable connection to the weakest. Bolted connections failing to one of the two conditions were not taken into account in this ranking.

Table 2.3 Ranking bolted connections

Type	Anchor length [mm]	Tensile [kN]	Shear [kN]	Bending [Nm]
1) Concrete Wedge anchor	54	16,5	10,6	21,7
2) Socket With bolt	65	16	8,0	/
3) Lag shield anchor	51	10,43	11,92	60
4) Screw anchor	<70	9,0	12,8	46
5) High load anchor	67	7,6	10,1	6,9
6) Anchor stud + styrene	65	6,6	8	17,1

Another characteristic of the bolted connections should be analysed before the best connection could be identified is the binding and insertion in the concrete. According to Table 2.3, the most suitable connection would be the concrete Wedge anchor. However, because of the mass production of the precast UHPFRC slabs, the most beneficial choice according to production and installation costs is the socket with bolt. For the installation of the remaining anchors, the concrete should be predrilled which would take a lot of time compared to the pre-embedded socket.

The second main advantage of the fixing socket is that it has the ability to enlarge its anchorage. A steel bar through the socket can be added in the same direction as the length of the concrete slab, perpendicular to tensile forces. This causes a better behaviour of the connection while subjected to tensile or shear forces compared to the other fasteners. When comparing the behaviour of mechanical and chemical anchors due to tensile forces, it occurs that chemical anchors damage the inner surface of the concrete more. This results in a final ranking, presented in Table 2.4.

Table 2.4 Final result

Type	Anchor length [mm]	Tensile [kN]	Shear [kN]	Bending [Nm]
1) Socket With bolt	65	16	8,0	/
2) Anchor stud + styrene	65	6,6	8	17,1
3) Concrete Wedge anchor	54	16,5	10,6	21,7
4) Lag shield anchor	51	10,43	11,92	60
5) Screw anchor	<70	9,0	12,8	46
6) High load anchor	67	7,6	10,1	6,9

2.4 Fixing socket with bolt

Former tests and a paper, Etude de brises soleil on béton fibre ultra haute performance (2015), have been made about this connection to the UHPFRC slabs. An experimental study has been carried out to investigate the actual tension resistance and the behaviour of the concrete in the contact area with the bolt.

2.4.1 Fixing Socket Pfeifer

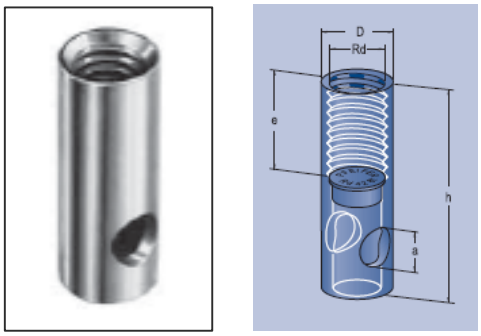

Figure 2.7 PFEIFER socket

The fixing socket was primarily designed as a lifting anchor. It consists of galvanized or stainless steel tube. Approximately a little more than the half of the tube is provided with a thread-system at the inside surface of the socket. The other part contains a plastic internal cap and a cross hole through the tube. A steel bar can be put through this hole as an extra reinforcements. If the socket is used as a lifting anchor, ropes or steel wires can be inserted.

2.4.2 Bolt hole

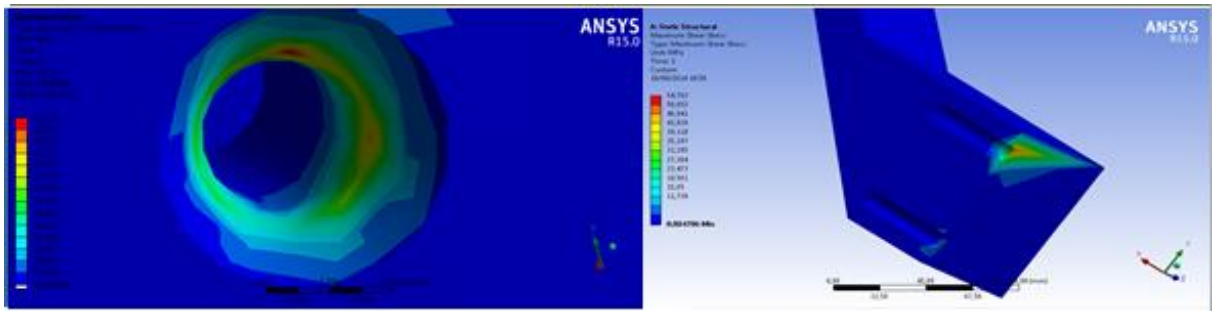

Figure 2.8 Model in ANSYS

The slab is connected to the framed structure by two metal connectors. Primarily, a structural calculation was made by the finite element method. This resulted in precautions to avoid stress concentration in the vicinity of the connectors and the external face of the prefabricated piece. Secondly, a computer simulated model was constructed in ANSYS to observe the stresses. In particular the outer face of the bolt hole suffers due to higher stress concentrations. This causes crumble of the concrete at the entrance of the bolt hole. Together with the experimental test, the model was adjusted and the conclusion was made to shape the bolt hole near the outer surface conical, as shown in Figure 2.8.

2.4.3 Tensile strength

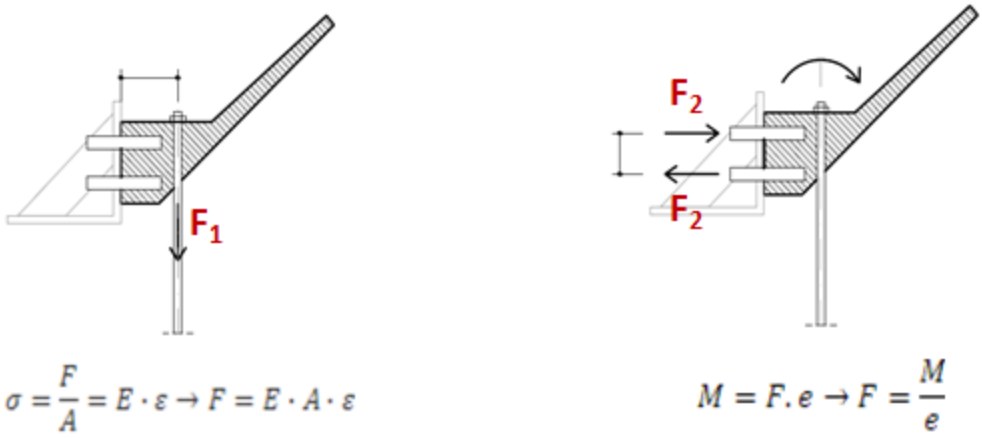

Figure 2.9 Connection slab with structure

Before the experimental tests, the capacity of tensile resistance of the connection was calculated. Theoretically, the connection could endure a maximum strain of 111,54 μs or 9,74kN. In order to obtain the maximum force, two strain gauges were applied on the connection and the maximum strain was measured. Because steel is known to be a linear material, hook's law can be used to convert the measured strain, 164,5μs, into a tensile resistance of 14,50kN which is sufficiently more than the calculated strength.

2.5 Conclusion

Mechanical and chemical bolted connections can fail due to static loads or dynamic loads. In the view of this thesis, the fixing socket with bolt is stated to be the best solution. To investigate the actual tensile strength and bonding to the concrete, static tests were carried out. Its behaviour subjected to cyclic loads, in particular fatigue failure, should be tested.

3 Wind

3.1 Characterization

3.1.1 Development

Energy from the sun is extracted by the earth and is given to the atmosphere which has a lower temperature. Regions of higher and lower temperatures will be initiated in the atmosphere causing large regions with a difference in air pressure. This latter phenomena excites wind flow from regions with a higher pressure to regions with a lower pressure.

A horizontal pressure difference could be caused due to solar radiation, humidity, rotation of the earth and surface cooling. This develops a pressure gradient or horizontal force determining the wind velocity and the direction of the motion of the wind. As the pressure gradient increases, the force on the air grows, resulting in a higher wind speed.

The rotation of the earth evokes variation in solar heating. Every morning, the sun heats the earth its surface and causes a temperature difference. The warmer parcels intend to rise and are subjected to an upwards acceleration until an layer with the same temperature is found. Colder parcels descend to take the first parcel its place and tend to have a higher horizontal velocity than the mean velocity of the parcels near the ground with which it mixes. When a parcel has a higher wind speed than the mean velocity, it is called a gust. Gusts are not only produced by thermal turbulence but by mechanical turbulence as well. This implies that a wind flow over the surface of the earth is influenced by the roughness and orography of the ground.

3.1.2 Variation in velocity

Variation in wind speed can be distinguished in three categories: Seasonal variation, daily variations and variations in very short periods, called gusts.

In many geographical areas, global winds are suffering from various different seasonal variations derived from solar radiation, the position of the anticyclones, depressions, etc. In fact, trends can be detected more or less according to cyclical variations depending on the seasons of the year. These are called the seasonal variations.

Daily variations are depending on the effects of heating or cooling from day or night, the proximity of the sea or the terrain orography. These characteristics result in many areas with cyclical wind variations. For example, coastal breezes or mountains.

In a short time, wind can suffer considerable variations in speed and direction. Defining gusts depends on the instantaneous wind speed from the average wind and on the duration of the gusts itself.

Gusts are divided in three categories:

Gust	: increase of wind speed with respect to the mean wind of 5-8 m/s.
Strong gust	: increase of wind speed with respect to the mean wind of 8-15 m/s.
Violent gust	: increase of wind speed with respect to the mean wind up to 15 m/s.

3.1.3 Estimation mean velocity

An estimation of the average wind speed in Marseille can be formed, based on the wind statistics which are represented in Figure 3.1. The annual mean velocity is identiefied as 11kts (knots). To convert this speed to km/h and m/s, it should be multiplied by 1,852 or 0,5144 respectively. The average velocity on ground level is 19,8km/h or 5,5m/s.

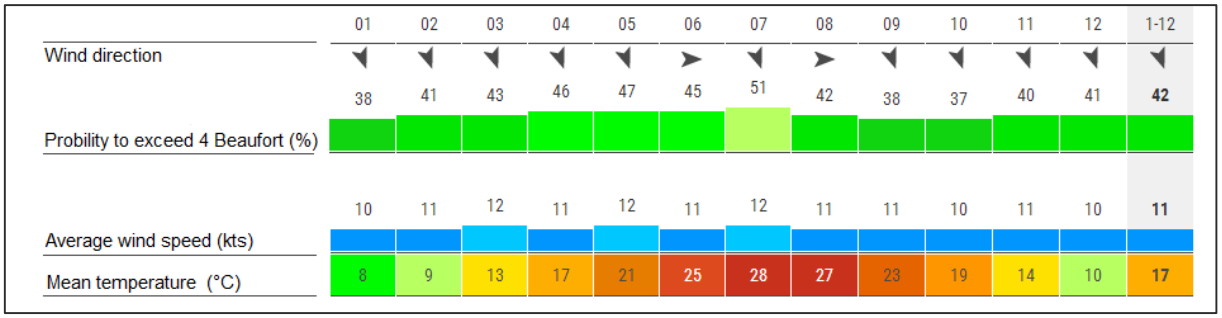

Figure 3.1 Wind statistics Marseille

The average speed can be compared to the Beaufort scale in Table 3.1. The 11kts wind in Marseille is equal to four Beaufort. This implies a moderate breeze. On landscape level this means that small branches of trees will move, leaves and paper can be uplifted, dust can be moved, etc.

Table 3.1 Beaufort Wind scale

Beaufort Wind Scale					
Beaufort Number or Force	Wind Speed			Description	Effects Land / Sea
	mph	km/hr	knots		
0	<1	<1	<1	Calm	Still, calm air, smoke will rise vertically. Water is mirror-like.
1	1-3 mph	1-5 kph	1-3 knots	Light Air	Rising smoke drifts, wind vane is inactive. Small ripples appear on water surface.
2	4-7 mph	6-11 kph	4-6 knots	Light Breeze	Leaves rustle, can feel wind on your face, wind vanes begin to move. Small wavelets develop, crests are glassy.
3	8-12 mph	12-19 kph	7-10 knots	Gentle Breeze	Leaves and small twigs move, light weight flags extend. Large wavelets, crests start to break, some whitecaps.
4	13-18 mph	20-28 kph	11-16 knots	Moderate Breeze	Small branches move, raises dust, leaves and paper. Small waves develop, becoming longer, whitecaps.
5	19-24 mph	29-38 kph	17-21 knots	Fresh Breeze	Small trees sway. White crested wavelets (whitecaps) form, some spray.
6	25-31 mph	39-49 kph	22-27 knots	Strong Breeze	Large tree branches move, telephone wires begin to "whistle", umbrellas are difficult to keep under control. Larger waves form, whitecaps prevalent, spray.
7	32-38 mph	50-61 kph	28-33 knots	Moderate or Near Gale	Large trees sway, becoming difficult to walk. Larger waves develop, white foam from breaking waves begins to be blown.
8	39-46 mph	62-74 kph	34-40 knots	Gale or Fresh Gale	Twigs and small branches are broken from trees, walking is difficult. Moderately large waves with blown foam.
9	47-54 mph	75-88 kph	41-47 knots	Strong Gale	Slight damage occurs to buildings, shingles are blown off of roofs. High waves (6 meters), rolling seas, dense foam, Blowing spray reduces visibility.
10	55-63 mph	89-102 kph	48-55 knots	Whole Gale or Storm	Trees are broken or uprooted, building damage is considerable. Large waves (6-9 meters), overhanging crests, sea becomes white with foam, heavy rolling, reduced visibility.
11	64-72 mph	103-117 kph	56-63 knots	Violent Storm	Extensive widespread damage. Large waves (9-14 meters), white foam, visibility further reduced.
12	73+ mph	118+ kph	64+ knots	Hurricane	Extreme destruction, devastation. Large waves over 14 meters, air filled with foam, sea white with foam and driving spray, little visibility.

3.2 Test conditions

3.2.1 Wind forces

Wind is affected by many variable parameters. To simulate the wind in the experiments conducted in chapter 4, some key issues should be defined. Therefore, the wind velocity and amplitude of the wind fluctuations or gust magnitude will be determined in the following paragraphs. Assumptions in the calculations for the main parameters are made in the in the purpose of the building discussed in paragraph 1.4.

The calculations in this paragraph are made according to EN 1991-1-4 (2005). Wind forces can be calculated by two different methods. The first calculation method is based on surface pressures, shown in Figure 3.2. While the second method uses force coefficients, represented in Figure 3.3. All parameters used, can be found in the nomenclature.

Two different cases should be considered according to the influence of the wind:

.- Frontal wind on the cladding.
The slab will be considered as a canopy with an inclination and the output of the wind is completely obstructed. When isolated canopies are considered, the combined effect of wind acting on the upper and lower surfaces should be taken into account.

.- Suction induced by wind on the opposite façade.
In this situation, a vertical wall is considered. The effect of the wind force perpendicular on the wall, will be projected on the inclined surface of the slab.

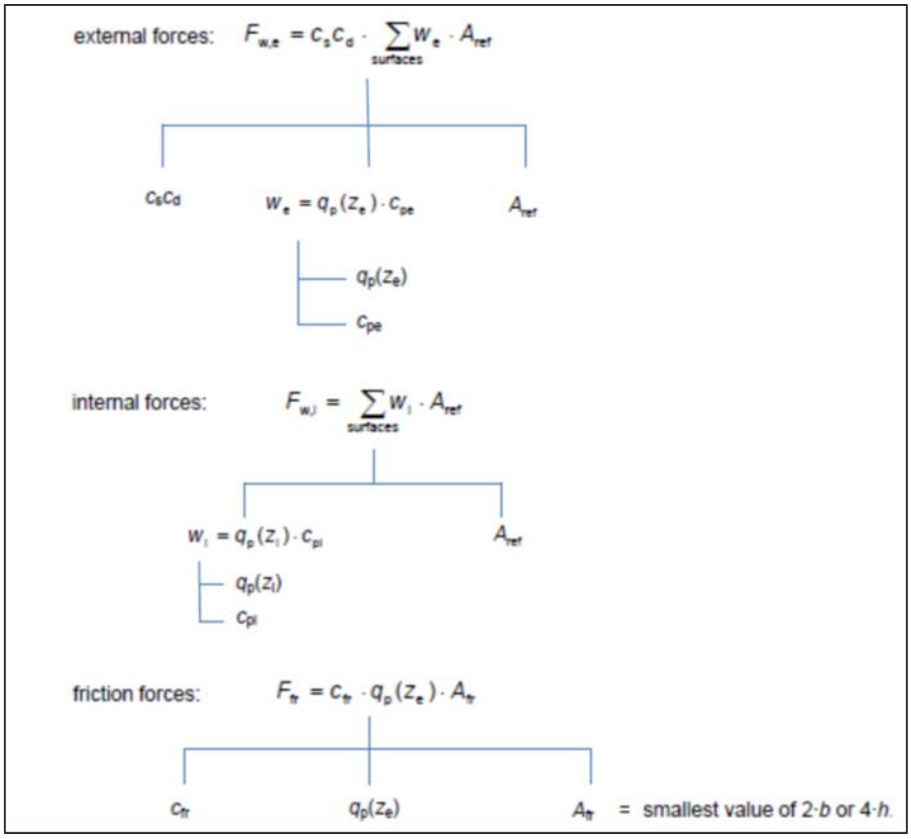

Figure 3.2 Flowchart Wind forces based on surface pressure according to EC 1.4

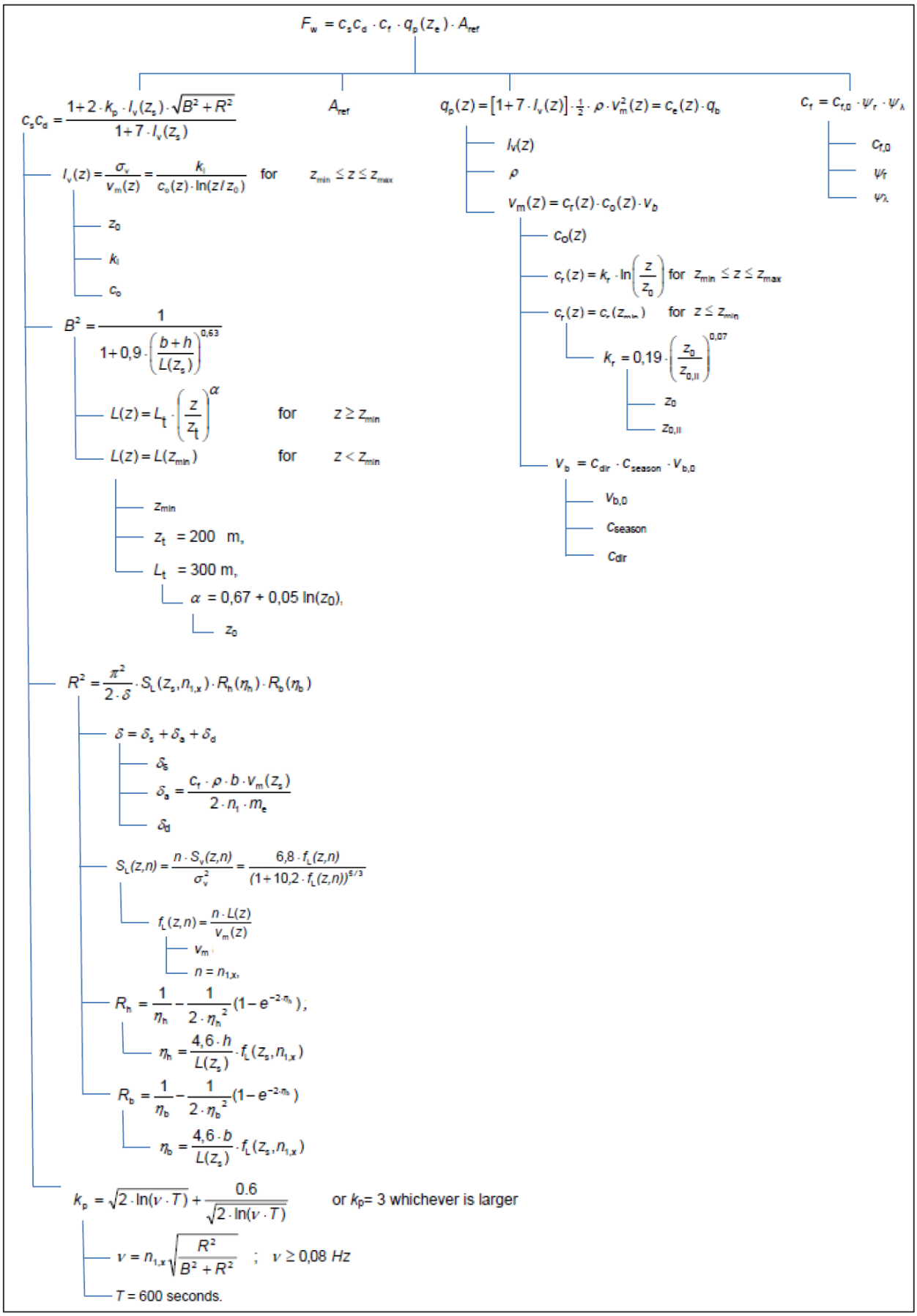

Figure 3.3 Flowchart Wind Forces based on force coefficients according to EC 1.4

3.2.1.1 Wind force calculation based on force coefficients

The total wind force, Fw, on structures or elements can be established by the combination of four parameters:

$$Fw = c_s c_d * c_f * q_p(z_e) * A_{ref} \quad (3.1)$$

$c_s c_d$ is the structural factor defined in paragraph 3.2.1.1.3
c_f represents the force coefficient for the structure (see 3.2.1.1.1)
$q_p(z_e)$ is the peak velocity pressure at reference height, z_e, discussed in paragraph 3.2.1.1.2
A_{ref} the reference area of the structure (see 3.2.1.1.1)

Assumed is that the maximum building height is 20m, in this case, z_e can be taken into account as the maximum height.

3.2.1.1.1 C_f and A_{ref}

A_{ref} is taken as the reference area, the blade length multiplied by its height. With length: b = 2850mm and height: h = 250mm. $\boldsymbol{A_{ref}}$ **= 0,7125m²**

c_f is the force coefficient for the structure or structural element expressed in (3.2):

$$c_f = c_{f,0} * \psi_r * \psi_\lambda \quad (3.2)$$

$c_{f,0}$, the force coefficient for structural elements with rectangular sections with sharp corners and without free-end flow should be used, given by Figure 3.4. Consideration: the value of $c_{f,0}$ is for the wind blowing perpendicular to one side. In the section of the bridge deck, it is possible that the wind blows on a non-perpendicular surface. With this consideration $c_{f,0}$ can reduce the wind pressure with 30%.

In this case is d = 250mm and b = 250mm→ $\boldsymbol{c_{f,0}} = 2{,}1 * 0{,}7 = \mathbf{1{,}47}$

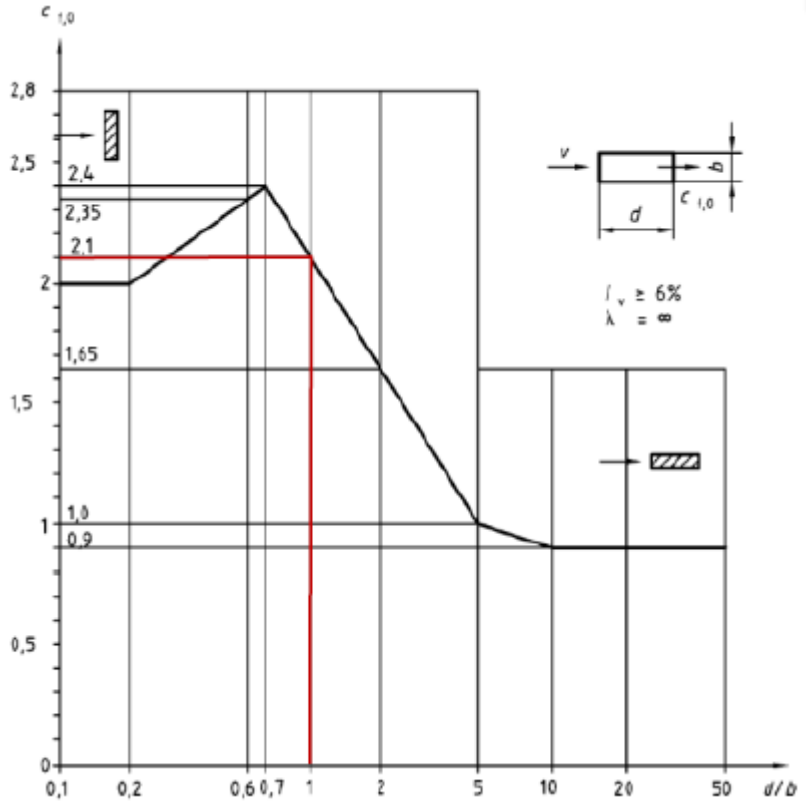

Figure 3.4 Force coefficient in function van d/b

ψ_r is the reduction factor for square sections with rounded corners. This factor should not be applied. Therefore, $\boldsymbol{\psi_r = 1,0}$.

ψ_λ is the end-effect factor for elements with free-end flow and depends on the slenderness of the structure, λ, given in Table 3.2, and the solidity ratio φ.
The structure has a rectangle. The length is 2,85m thus less than 15m. l/b = 2,85/0,05 = 57.
Therefore expression (3.3) should be used and thus $\boldsymbol{\lambda = 70}$.

$$\lambda = \min\{2 * l/b\ ; 70\ \} \tag{3.3}$$

Table 3.2 Recommended values of the slenderness

No.	Position of the structure, wind normal to the plane of the page	Effective slenderness λ
1	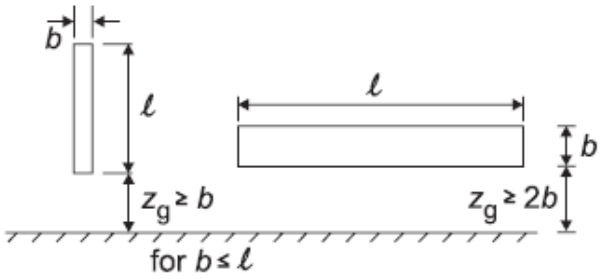	For polygonal, rectangular and sharp edged sections and lattice structures: for $\ell \geq 50$ m, $\lambda = 1{,}4\ \ell/b$ or $\lambda = 70$, whichever is smaller
2	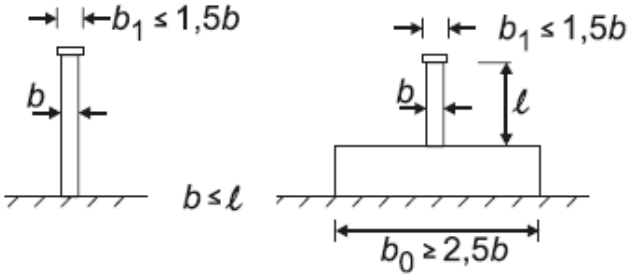	for $\ell < 15$ m, $\lambda = 2\ \ell/b$ or $\lambda = 70$, whichever is smaller For circular cylinders: for $\ell \geq 50$, $\lambda = 0{,}7\ \ell/b$ or $\lambda = 70$, whichever is smaller for $\ell < 15$ m, $\lambda = \ell/b$ or $\lambda = 70$, whichever is smaller
3	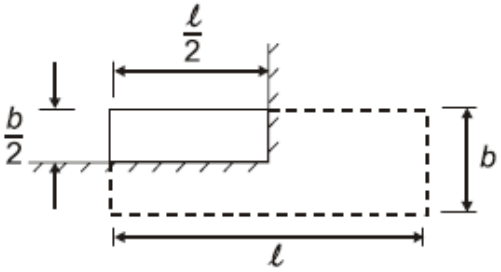	For intermediate values of ℓ, linear interpolation should be used
4	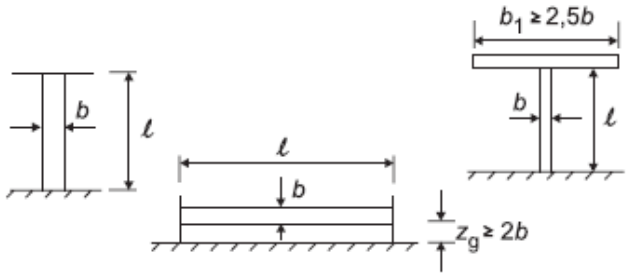	for $\ell \geq 50$ m, $\lambda = 0{,}7\ \ell/b$ or $\lambda = 70$, whichever is larger for $\ell < 15$ m, $\lambda = \ell/b$ or $\lambda = 70$, whichever is larger For intermediate values of ℓ, linear interpolation should be used

The solidity ratio φ is known as the fraction of the sum or the projected areas of the members to the overall envelope area. In other words, ratio of surface area exposed to the wind and the total area. Here it can considered as equal which results in φ = 1.

ψ_λ can be found in Figure 3.5. $\boldsymbol{\psi_\lambda}$ **= 0,92.**

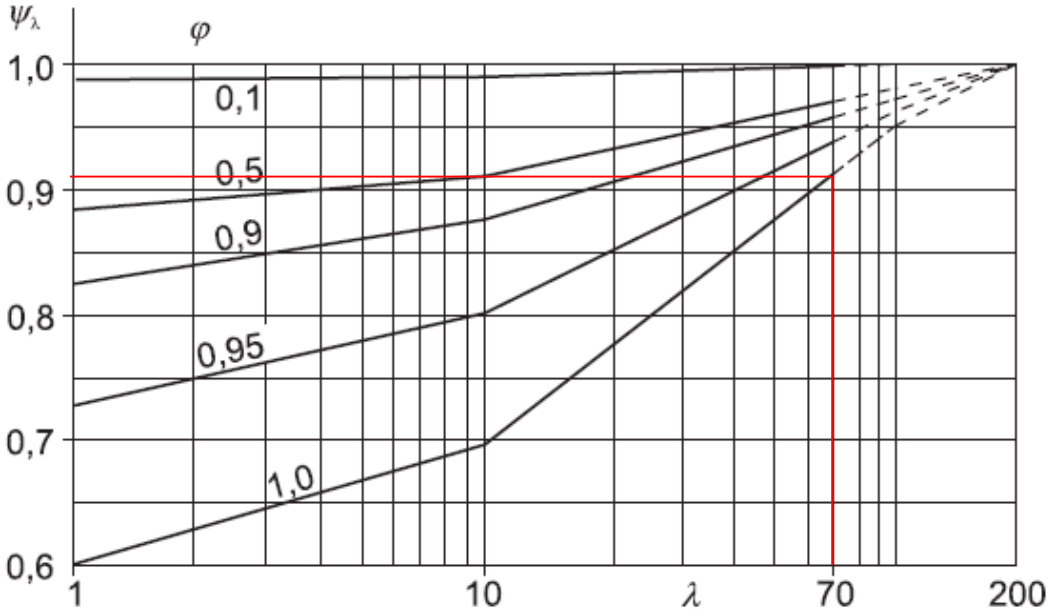

Figure 3.5 Values of the end-effect in function of the solidity ratio versus the slenderness

This means according to expression (3.2) that $\boldsymbol{c_f = 1,3524}$

Table 3.3 Parameters and results of cf

Parameters	Results
$c_{f,0}$	1,47
ψ_r	1
ψ_λ	0,92
c_f	**1,3524**

3.2.1.1.2 Peak velocity pressure, $q_p(z_e)$

The parameter $q_p(z_e)$ is characterized by the terrain category with corresponding factors and by the wind climate at a certain reference height z_e and can be calculated by two different approaches.

$$q_p(z_e) = [1 + 7 * Iv(z)] * \frac{1}{2} * \rho * v_m^2(z) = c_e(z) * q_b \quad (3.4)$$

$\boldsymbol{\rho}$ is the air density, the recommended value in the National Annex is **1,225 kg/m³**. $Iv(z)$ is the turbulence intensity expressed in (3.5). The wind velocity, $v_m(z)$ at a height z above the terrain is obtained in expression (3.6).

$Iv(z)$ represents the turbulence intensity at height z and is influenced by terrain parameters which depend on the terrain category:

$$Iv(z_s) = \frac{\sigma_v}{v_m(z)} = \frac{k_1}{c_0(z) * \ln(z/z_0)} \qquad for\ z_{min} \le z \le z_{max} \quad (3.5)$$

$$Iv(z) = Iv(z_{min}) \qquad for\ z \le z_{min}$$

$\boldsymbol{k_1}$ is the turbulence factor. This factor can be found in the National annex if not, the recommended value is **1,0.**

$\boldsymbol{c_0(z)}$ is the orography factor. Supposing that the terrain is flat (no hills or cliffs present that can increase the wind velocities) the effects of the orography can be disregarded and $c_0(z)$ is taken into account as **1,0**.

z_{max} should be taken as 200m. The reference height z is equal to 20m.

z_0, the roughness length and z_{min}, minimum height are defined in Table 3.4. Assumed is the terrain category 0 because Marseille is situated at the Mediterranean Sea. Thus, $\boldsymbol{z_0}$ = **0,005** and $\boldsymbol{z_{min}}$= **1**. This means $z_{min} \leq z \leq z_{max} = 1m \leq 20m \leq 200m \rightarrow \boldsymbol{Iv(z_s) = 0,1669}$.

Table 3.4 Terrain categories with parameters according to the National annex of France

Catégorie de terrain		z_0 [m]	z_{min} [m]
0	Mer ou zone côtière exposée aux vents de mer ; lacs et plans d'eau parcourus par le vent sur une distance d'au moins 5 km	0,005	1
II	Rase campagne, avec ou non quelques obstacles isolés (arbres, bâtiments, etc.) séparés les uns des autres de plus de 40 fois leur hauteur	0,05	2
IIIa	Campagne avec des haies ; vignobles ; bocage ; habitat dispersé	0,20	5
IIIb	Zones urbanisées ou industrielles ; bocage dense ; vergers	0,5	9
IV	Zones urbaines dont au moins 15 % de la surface sont recouverts de bâtiments dont la hauteur moyenne est supérieure à 15 m ; forêts	1,0	15
NOTE 1 Les catégories de terrain sont illustrées par les photographies aériennes des figures 4.6(NA) à 4.14(NA). NOTE 2 Le coefficient de rugosité, fonction de la catégorie de terrain et de la hauteur *z*, est illustré à la figure 4.15(NA).			

The mean wind velocity depends on various parameters:

$$v_m(z) = c_r(z) * c_0(z) * v_b \tag{3.6}$$

$c_r(z)$ is the roughness factor is taken into account because of the variability of the wind speed at the site due to the height above to terrain and the terrain roughness:

$$c_r(z) = k_r * \ln(z/z_0) \qquad for\ z_{min} \leq z \leq z_{max} \tag{3.7}$$

$$c_r(z) = c_r(z_{min}) \qquad for\ z \leq z_{min}$$

k_r is the terrain factor, calculated by using expression (3.8) with $z_{0,II}$ equal to the roughness length of terrain category II (Table 3.4).

$$k_r = 0{,}19 * \left(\frac{z_0}{z_{0,II}}\right)^{0,07} \tag{3.8}$$

$\boldsymbol{k_r = 0,1617}$ which gives for $\boldsymbol{c_r(20)}$ = **1,3413**.

$c_0(z)$ is the orography factor. This factor was previously determined: $\boldsymbol{c_0(z) = 1}$

v_b is the basic wind speed, see expression (3.9), and depends on the wind climate (seasonal and directional effects) on a terrain with terrain category II:

$$v_b = c_{dir} * c_{saeson} * v_{b,0} \tag{3.9}$$

$\boldsymbol{c_{dir}}$is the directional factor and is taken into account with a value equal **to 1,0.**

$\boldsymbol{c_{saeson}}$ is the seasonal factor with a recommended factor **of 1,0.**

$v_{b,0}$ is the fundamental value of the basic wind velocity. EN 1991-1-4 (2005) states: "$v_{b,0}$ is the characteristic 10 minutes mean wind velocity, irrespective of wind direction and time of year, at 10 m above ground level in open country terrain with low vegetation such as grass and isolated obstacles with separations of at least 20 obstacle heights." The fundamental wind speed depends on the wind zone where the structure is situated, shown in Table 3.5. Marseille is situated in department 13: Bouchee-du-Rhone which results in wind zone 3. In Figure 3.6, the zones and their corresponding fundamental basic wind velocity is giving: $\boldsymbol{v_{b,0} = 26\ m/s}$ for zone 3.

By using expression (3.9), this gives a value of **26 m/s for v_b** which results with the roughness and orography factor into a mean speed velocity, $\boldsymbol{v_m(20)}$ **= 34,8738 m/s.**

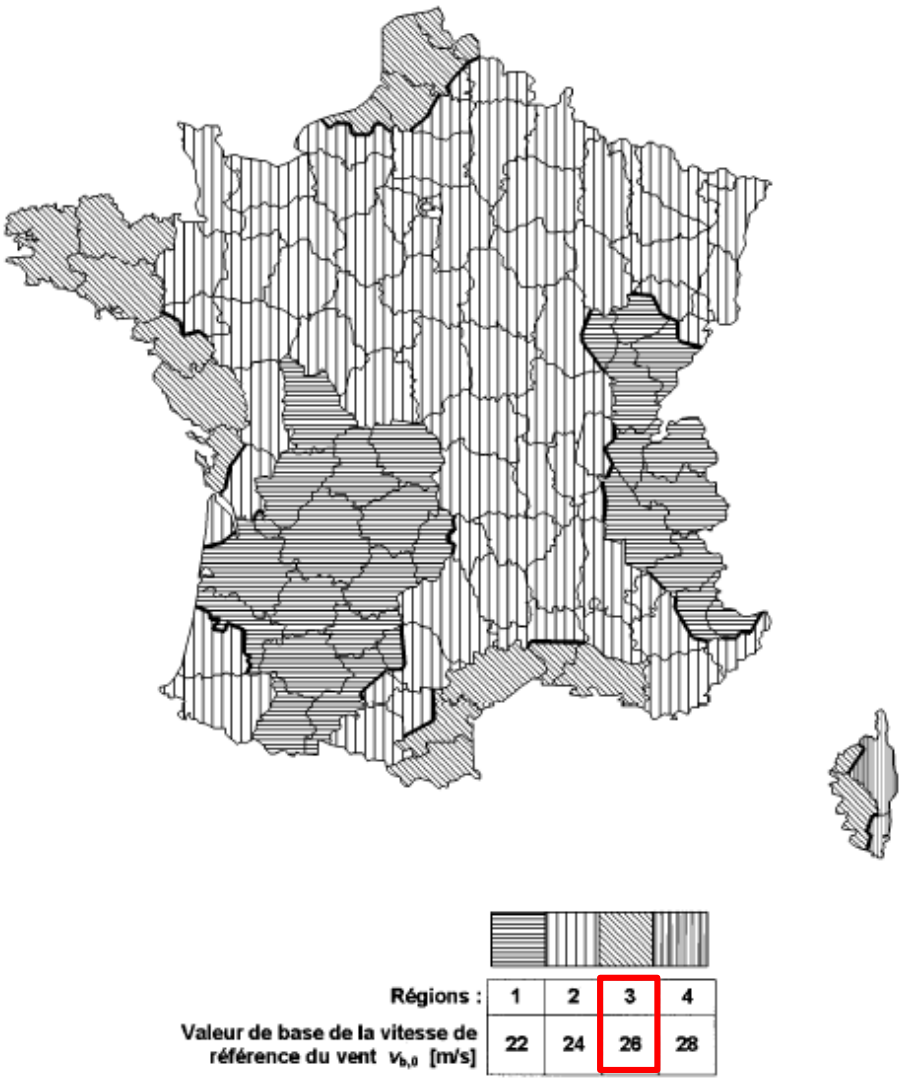

Figure 3.6 Classification of the wind zones accompanied by the fundamental wind speed

Table 3.5 Classification of the wind zones

Département	Région(s)	Département	Région(s)	Département	Région(s)
01 Ain	1 ; 2	32 Gers	1	64 Pyrénées-Atlantiques	2
02 Aisne	2	33 Gironde	1 ; 2	65 Hautes-Pyrénées	1
03 Allier	2	34 Hérault	3	66 Pyrénées-Orientales	3
04 Alpes-de-Haute-Provence	1 ; 2	35 Ille-et-Vilaine	2	67 Bas-Rhin	2
05 Hautes-Alpes	1 ; 2	36 Indre	2	68 Haut-Rhin	2
06 Alpes-Maritimes	1 ; 2	37 Indre-et-Loire	2	69 Rhône	2
07 Ardèche	2	38 Isère	1 ; 2	70 Haute-Saône	1 ; 2
08 Ardennes	2	39 Jura	1	71 Saône-et-Loire	2
09 Ariège	2	40 Landes	1 ; 2	72 Sarthe	2
10 Aube	2	41 Loir-et-Cher	2	73 Savoie	1
11 Aude	2 ; 3	42 Loire	2	74 Haute-Savoie	1
12 Aveyron	2	43 Haute-Loire	2	75 Paris	2
13 Bouches-du-Rhône	3	44 Loire-Atlantique	2 ; 3	76 Seine-Maritime	2 ; 3
14 Calvados	2	45 Loiret	2	77 Seine-et-Marne	2
15 Cantal	1 ; 2	46 Lot	1	78 Yvelines	2
16 Charente	1	47 Lot-et-Garonne	1	79 Deux-Sèvres	2
17 Charente-Maritime	1 ; 2 ; 3	48 Lozère	2	80 Somme	2 ; 3
18 Cher	2	49 Maine-et-Loire	2	81 Tarn	1 ; 2
19 Corrèze	1	50 Manche	2	82 Tarn-et-Garonne	1
2B Haute-Corse	3 ; 4	51 Marne	2	83 Var	2
2A Corse-du-Sud	3 ; 4	52 Haute-Marne	2	84 Vaucluse	2
21 Côte-d'Or	1 ; 2	53 Mayenne	2	85 Vendée	3
22 Côtes-d'Armor	3	54 Meurthe-et-Moselle	2	86 Vienne	1
23 Creuse	1	55 Meuse	2	87 Haute-Vienne	1
24 Dordogne	1	56 Morbihan	3	88 Vosges	2
25 Doubs	1 ; 2	57 Moselle	2	89 Yonne	2
26 Drôme	2	58 Nièvre	2	90 Territoire de Belfort	2
27 Eure	2	59 Nord	2 ; 3	91 Essonne	2
28 Eure-et-Loir	2	60 Oise	2	92 Hauts-de-Seine	2
29 Finistère	3	61 Orne	2	93 Seine-Saint-Denis	2
30 Gard	2 ; 3	62 Pas-de-Calais	2 ; 3	94 Val-de-Marne	2
31 Haute-Garonne	1 ; 2	63 Puy-de-Dôme	2	95 Val-d'Oise	2

Combining the different parameters and inserting them expression (3.4): $q_p(z_e) = 1,614$ **[kN/m²].**

Table 3.6 Parameters and results of qp(ze)

Parameters	Results
$Iv(z_s)$	0,1667
ρ [kg/m³]	1,225
$v_m(z_s)$ [m/s]	34,8738
$q_p(z_e)$ **[kN/m²]**	**1,614**

The second approach for the calculation of $q_p(z_e)$, by determining the right part of expression (3.4): $q_p(z_e) = c_e(z) * q_b$.

q_b is known as the velocity pressure. The basic wind velocity, v_b, and the air density, ρ, has been previously assumed. Therefore $\boldsymbol{q_b = 414,05}$ **N/m².**

$$q_b = \frac{1}{2} * \rho * {v_b}^2 \tag{3.10}$$

$c_e(z)$ is the exposure factor. This factor is captured in five different graphics according to the terrain categories. For a reference height of 20m and terrain category 0, the exposure factor is: $c_e(z) = 3{,}4$.

This indicates that $\boldsymbol{q_p(z_e) = 1,4078\ kN/m^2}$

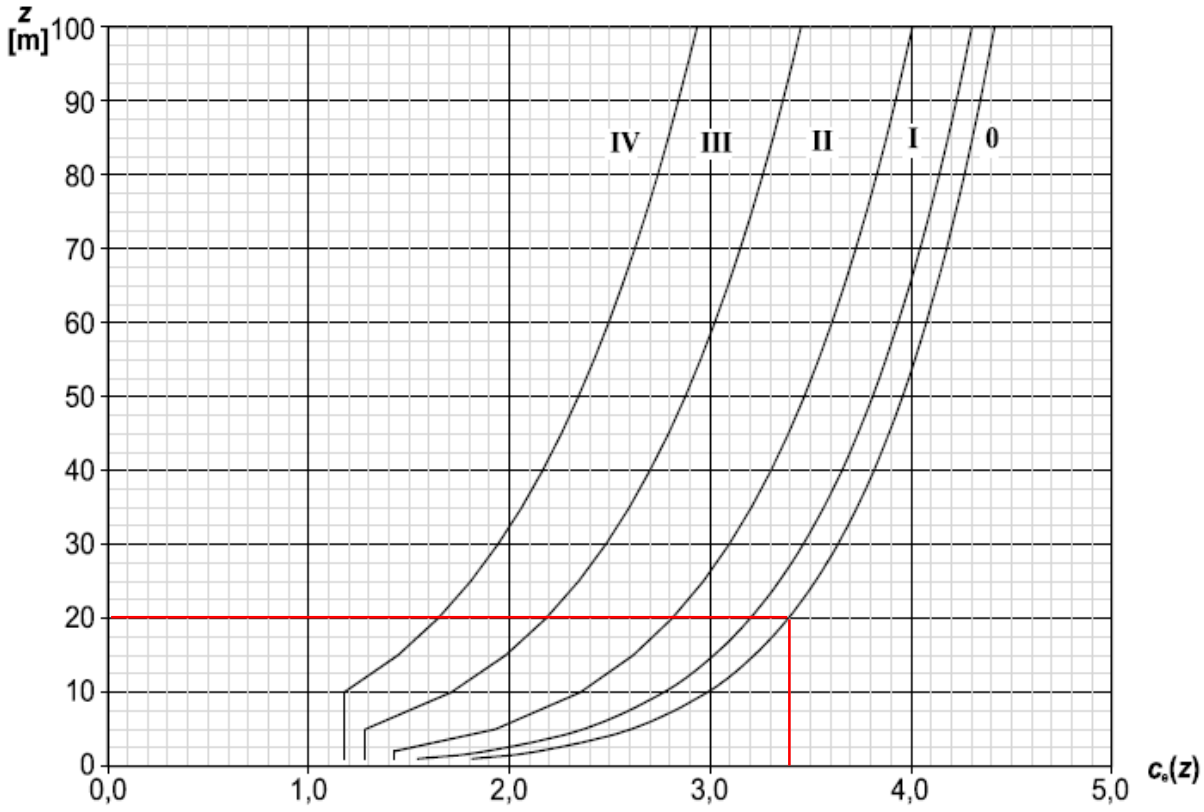

Figure 3.7 Exposure factor in function of terrain category and height

3.2.1.1.3 Structural factor, $c_s c_d$

The structural factor could be divided in two effects: "The effect on wind actions from the non-simultaneous occurrence of peak wind pressures on the surface (c_s) together with the effect of the vibrations of the structure due to turbulence (c_d)."

$$c_s c_d = \frac{1 + 2 * k_p * Iv(z_s) * \sqrt{B^2 + R^2}}{1 + 7 * Iv(z_s)} \tag{3.11}$$

With k_p, the peak factor determined in expression (3.21), $Iv(z_s)$, the turbulence intensity obtained in expression (3.5), z_s, the reference height (20m), B^2, the background factor defined in expression (3.12) and R^2, the resonance response factor (3.14).

The background factor is used to bring the lack of correlation of the wind gusts over the structure surface into account and is expressed by the following calculation:

$$B^2 = \frac{1}{1 + 0{,}9 * (\frac{b+h}{L(z_s)})^{0{,}63}} \tag{3.12}$$

b and h, the width and the height of the concrete slab exposed to wind, 2850mm and 250mm respectively. L(z_s) is the turbulent length scale which represents the mean gust size for naturally occurring winds. For heights z lower then 200m, the turbulent length scale could be defined by using:

$$L(z_s) = L_t * (\frac{z}{z_t})^{\alpha} \tag{3.13}$$

z_t is the reference height for L_t and is equal to 200m. L_t is a reference length scale of 300m.
$\alpha = 0{,}67 + 0{,}05\ln(z_0) = 0{,}3795$. Which gives $L(z_s) = 125{,}193m \rightarrow$ $\boldsymbol{B^2 = 0{,}9195.}$

R^2 known as the resonance factor, should be calculated by:

$$R^2 = \frac{\pi}{2\delta} * S_L(z_s, n_{1,x}) * R_h(\eta_h) * R_b(\eta_b) \tag{3.14}$$

δ is the total logarithmic decrement of damping, S_L is the non-dimensional power spectral density function and R_h, R_b are the aerodynamic admittance functions.

The logarithmic decrement of damping δ may be estimated for the fundamental bending by:

$$\delta = \delta_s + \delta_a + \delta_d \tag{3.15}$$

δ_s is the logarithmic decrement of structural damping. Approximate values of δ_s are given in Table 3.7. In this case the δ_s should be exerted on a concrete bridge with cracks. The value of $\boldsymbol{\delta_s = 0.10}$

δ_d is the logarithmic decrement of damping due to special devices (tuned mass dampers, sloshing tanks etc.). There are damping devices present: $\delta_d = 0$.

δ_a is the logarithmic decrement of aerodynamic damping for the fundamental mode which depends on the mass per unit area of the structure and modal deflections. Because of the fact that model deflections (in most cases) are constant for a certain height, the natural fundamental frequency of the structure, n_1, could be used in combination with the mass per unit length:

$$\delta_a = \frac{c_f * \rho * b * v_m(z_s)}{2 * n_1 * m_e} \tag{3.16}$$

n_1 is the frequency corresponding to mode 1. EN 1991-1-4 (2005) does not provide an expression to calculate n_1 for the UHPFRC slabs. Therefore numerical data obtained from tests((Llorens, 2015) will be used. $n_1 = 22{,}41$Hz shown in Table 3.8.

m_e is the equivalent mass = 66,408 kg. (value from experimental study (Llorens, 2015))
$v_m(z_s)$ wind velocity calculated with expression (3.6) = 34,8738 m/s.
ρ is the air density = 1,225 kg/m³.
b is the length of the slab = 2850 mm.
$\boldsymbol{c_f}$ is the force coefficient determined in paragraph 3.2.1.1.1 with a value of 1,3524.

Table 3.7 Approximate values of δs

Structural type		**structural damping, δ_s**
reinforced concrete buildings		0,10
steel buildings		0,05
mixed structures concrete + steel		0,08
reinforced concrete towers and chimneys		0,03
unlined welded steel stacks without external thermal insulation		0,012
unlined welded steel stack with external thermal insulation		0,020
steel stack with one liner with external thermal insulation[a]	$h/b < 18$	0,020
	$20 \leq h/b < 24$	0,040
	$h/b \geq 26$	0,014
steel stack with two or more liners with external thermal insulation [a]	$h/b < 18$	0,020
	$20 \leq h/b < 24$	0,040
	$h/b \geq 26$	0,025
steel stack with internal brick liner		0,070
steel stack with internal gunite		0,030
coupled stacks without liner		0,015
guyed steel stack without liner		0,04
steel bridges + lattice steel towers	welded	0,02
	high resistance bolts	0,03
	ordinary bolts	0,05
composite bridges		0,04
concrete bridges	prestressed without cracks	0,04
	with cracks	0,10
Timber bridges		0,06 - 0,12
Bridges, aluminium alloys		0,02
Bridges, glass or fibre reinforced plastic		0,04 - 0,08
cables	parallel cables	0,006
	spiral cables	0,020
NOTE 1 The values for timber and plastic composites are indicative only. In cases where aerodynamic effects are found to be significant in the design, more refinded figures are needed through specialist advice (agreed if appropriate with the competent Authority. NOTE 2 For cable supported bridges the values given in Table F.2 need to be factored by 0,75		
[a] For intermediate values of h/b, linear interpolation may be used		

Inserting all parameters in expression (3.16) gives for $\delta_a = 0{,}055321$.
With $\delta_a = 0{,}055321$, $\delta_d = 0$ and $\boldsymbol{\delta_s}$ **=** 0,10:
$\boldsymbol{\delta = 0{,}1553}$

Table 3.8 Numerical and experimental frequencies

COMPARISON DES FREQUENCES FONDAMENTALES						
FREQUENCE	NUMERIQUES		EXPERIMENTALES			% erreur
	Fréquence (Hz)	Type du mode	Fréquence (Hz)	amortissement (%)	Type du mode	
Première	22.41	1 F	29.61	2.18	1 F	30.23
Deuxième	47.96	2 F	47.91	0.56	2 F	0,10
Troisième	86.80	1 T	87.52	0.73	1 T	0.82
Quatrième	91.77	2 T	94.29	3.52	2 T	2.67
Cinquième	113.32	3 T	110.06	0.86	3 T	2.85
Sixième	152.91	4 F	154.28	0.55	4 F	0.89
Septième	166,19	3T	186.09	0.39	3T	---

The wind velocity distributed over different frequencies is expressed as $S_L(z_s, n_{1,x})$, the non-dimensional power spectral density function, determined by using expression (3.17):

$$S_L(z_s, n_{1,x}) = \frac{n * S_v(z,n)}{\sigma_v^2} = \frac{6{,}8 * f_l(z,n)}{\left(1 + 10{,}2 * f_l(z,n)\right)^{5/3}} \tag{3.17}$$

Hereby is $S_v(z,n)$ is the one-sided variance spectrum.
$f_L(z,n)$ is a non-dimensional frequency, depending on the eigenfrequency of the structure, the turbulence length scale, $L(z)$ =125,2 m and the average wind speed, $v_m(z)$ =35,73 m/s:

$$f_L(z,n) = \frac{n * L(z)}{v_m(z)} \tag{3.18}$$

These factors were previously discussed. Thus, $f_L(z,n) = 80{,}4539$
$\boldsymbol{S_L(z_s, n_{1,x}) = 0{,}00759}$

$R_h(\eta_h)$ and $R_b(\eta_b)$, the aerodynamic admittance functions for a fundamental vibration mode may be approximated by using expressions (3.19)and (3.20) with h = 0,25m and b = 2,85m:

$$R_h(\eta_h) = \frac{1}{\eta_h} - \frac{1}{2 * \eta_h^2}(1 - e^{-2*\eta_h}) \quad with \quad \eta_h = 4{,}6 * \frac{h}{L(z_s)} * f_L(z_s, n_{1,x}) \tag{3.19}$$

$$and \;\; R_h = 1 \; for \; \eta_h = 0$$

$$R_b(\eta_b) = \frac{1}{\eta_b} - \frac{1}{2 * \eta_b^2}(1 - e^{-2*\eta_b}) \quad with \quad \eta_b = 4{,}6 * \frac{b}{L(z_s)} * f_L(z_s, n_{1,x}) \tag{3.20}$$

$$and \;\; R_b = 1 \; for \; \eta_b = 0$$

$\eta_h = 0{,}7390$
$\eta_b = 8{,}4245$

$\boldsymbol{R_h = 0,6465}$
$\boldsymbol{R_b = 0,1117}$

With previously become values, expression (3.14) is equal to: $\boldsymbol{R^2}$ **= 0,005548**

k_p is defined by the parameters v, the up-crossing frequency obtained by expression (3.22) and T, the averaging time for the mean wind velocity = 600 seconds, in expression (3.21):

$$k_p = \max\{\sqrt{2 * \ln(v * T)} + \frac{0.6}{\sqrt{2 * \ln(v * T)}}\ ; 3\} \tag{3.21}$$

$$v = n_{1,x}\sqrt{\frac{R^2}{B^2 + R^2}} \tag{3.22}$$

$v =$ 1,7355 → $\boldsymbol{k_p}$ = **3,8887**

With the parameters collected in Table 3.9, the structural factor can be calculated with expression (3.11) : $\boldsymbol{c_s c_d}$ **= 1,0367**.

Table 3.9 Parameters and results of CsCd

Parameters	Results
$\boldsymbol{Iv(z_s)}$	0,1669
$\boldsymbol{B^2}$	0,9195
$\boldsymbol{R^2}$	0,005548
$\boldsymbol{k_p}$	3,8887
$\boldsymbol{c_s c_d}$	**1,0367**

3.2.1.1.4 Total wind Force

According to expression (3.1), the total wind force should be:
$Fw = c_s c_d * c_f * q_p(z_e) * A_{ref}$ = 1,0367 * 1,3524 * 1,614 * 0,7125 = 1,623 kN.

Table 3.10 Resulting wind force

Parameters	Results
$\boldsymbol{c_s c_d}$	1,0367
$\boldsymbol{c_f}$	1,3524
$\boldsymbol{q_p(z_e)}$ **[kN/m²]**	1,614
$\boldsymbol{A_{ref}}$ **[m²]**	0,7125
$\boldsymbol{Fw}$ **[kN]**	**1,6123**

3.2.1.2 Wind force calculation based on surface pressure

A second method to calculate wind force is the summation of external, internal and friction forces with their expressions based on pressure coefficients:

$$F_w = F_{w,e} + F_{w,i} + F_{fr} \tag{3.23}$$

3.2.1.2.1 External forces, $F_{w,e}$

$$F_{w,e} = C_s C_d * \sum w_e * A_{ref} \tag{3.24}$$

$C_s C_d$ is structural factor, discussed and calculated in paragraph 3.2.1.1.3, $C_s C_d = 1{,}0367$
A_{ref} is the reference area, determined in paragraph 3.2.1.1.1, $\boldsymbol{A_{ref}}$ **= 0,7125m²**
w_e is the external pressure at height z_e, depending on the external pressure coefficient, C_{pe} and the peak velocity pressure at that height:

$$w_e = q_p(z_e) * C_{pe} \tag{3.25}$$

$q_p(z_e)$ has been approached by two different ways. The first approach will be used for the calculations because it is the most negative value thus: $q_p(z_e) = 1{,}614 kN/m^2$.

To be able to define C_{pe}, some considerations should be made:

- The concrete slabs behave like an insulated roof and is situated in zone A. Although the angle of the roof is greater than indicated in the table, the value of C_{pe} is descending.
- Coefficients of the overall strength (C_f) and net pressure ($C_{p,net}$) reflect the combined effect of wind acting on both the upper and lower surfaces
- Degree of total blockage (φ = 1).

In the paper, Etude de brises soleil en beton fibre ultra haute performance (Llorens, 2015) C_{pe}-factor was determined as -1,60 for frontal wind and -0,49 for wind on the opposite façade.

C_{pe} = -1,60 and $q_p(z_e) = 1{,}614 kN/m^2 \rightarrow w_{e,1} = 2{,}593\ kN/m^2$.
C_{pe} = -0,49 and $q_p(z_e) = 1{,}614 kN/m^2 \rightarrow w_{e,2} = 0{,}79086\ kN/m^2$.

Worst case: C_{pe} = -1,60 $\rightarrow$ $\boldsymbol{F_{w,e}}$ **= 1,9075** $\boldsymbol{kN}$**.**

3.2.1.2.2 Internal forces, $F_{w,i}$

$$F_{w,i} = \sum w_i * A_{ref} \tag{3.26}$$

A_{ref} is the reference area, determined in paragraph 3.2.1.1.1, $\boldsymbol{A_{ref}}$ **= 0,7125m²**
w_i is the internal pressure at height z_i, depending on the internal pressure coefficient, C_{pi} and the peak velocity pressure at that height. w_i = 0,70 (Llorens, 2015).

$\boldsymbol{F_{w,i}}$ **= 0,49875** $\boldsymbol{kN}$**.**

3.2.1.2.3 Friction forces, F_{fr}

$$F_{fr} = c_{fr} * q_p(z_e) * A_{fr} \quad (3.27)$$

Noted in EN 1991-1-4 (2005) is that for elements, the total wind force should be taken as the difference between the total of the external and the resulting internal forces. Friction forces can be neglected.

3.2.1.2.4 Resulting wind force

In paragraph 3.2.1.1 all the values and parameters are defined for the calculation of the wind force, F_w. In paragraph 3.2.1.2: expression (3.23) is converted to (3.28) when the considerations are applied:

$$F_w = F_{w,e} + F_{w,i} \quad (3.28)$$

This results in $F_w = F_{w,e} + F_{w,i}$ = 1,9075 + 0,49875 = 2,41kN.

3.2.1.3 Partial conclusion

The wind force based on force coefficients was calculated as 1,623kN. This is 0,8kN less than wind force based on pressure coefficients (2,41kN). The biggest value should be used for safety reasons when wind forces are simulated and the pressure should be applied on the entire blade. Equally important is the mean wind velocity determined in expression (3.6) equal to 34,87 m/s.

3.2.2 Gusts

Wind is divided in four components when it is modelled for a numerical test, Figure 3.8.

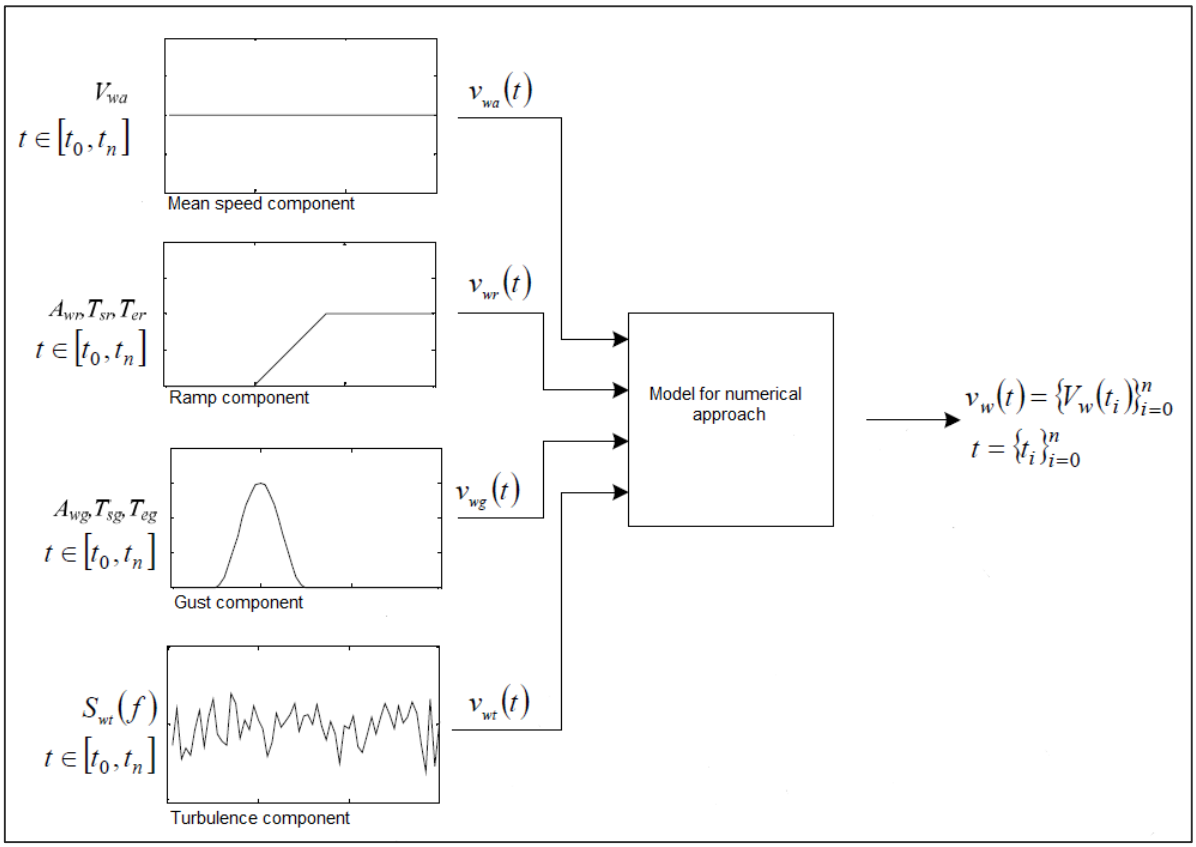

Figure 3.8 Components for numerical approach (Amaya, Cooz, Gonzalez-Longatt, & Duran, 2012)

The mean speed and ramp component represent the static part of wind forces. The gust component and turbulence component are the dynamic loads of the wind. Fatigue appears under dynamic loads, therefore only the last two components should be taken into account. In our case, the effect of gusts is tested. A gust of wind is characterized by using three different parameters:
.- Amplitude of the gust (A_g) in m/s.
.- start time of the gust (T_{sg}) in s.
.- completion time of the gust (T_{eg}) in s.

Before the fatigue test can be performed, the vertical displacement must be defined by using ANSYS Workbench 15.0 and Solidworks 2013. The displacement can be seen as the amplitude or the gust magnitude. As first, the bolted connection is constructed in Solidworks, shown in Figure 3.10. The concrete slab is reduced to 30cm of the original piece because only this length will be tested with a hydraulic pump. The Solidworks-model is inserted in ANSYS Workbench along with the characteristics of the concrete and steel determined in previous tests (Llorens, 2015), found in Table 3.11.

Table 3.11 Characteristics steel and concrete

Property	Value for steel	Value for concrete
Density [ton/mm^3]	7,85 E-09	2,6 * E-09
Coefficient of thermal expansion [$°C^{-1}$]	1,2*E-05	1,4*E-05
Reference temperature [$°C$]	22	22
Young's Modulus [MPa]	2*E+05	36370
Poisson's ratio	0,3	0,3
Tensile Ultimate Strength [MPa]	250	0
Compressive Yield Strength [MPa]	250	0
Tensile Ultimate Strength [MPa]	460	8
Compressive Ultimate Strength [MPa]	0	80

An alternating stress curve, should be added for the concrete. In the x-axis the number of loading cycles (N) is given, the y-axis contains the alternating stress amplitude (S). There is no graphic available, therefore an estimated curve is invented, refer to Figure 3.9. For example, when an alternating stress of 200MPa is applied, a specimen will fail due to fatigue after 450 cycles. An error has occurred while inventing the S-N curve. If a bigger stress amplitude is applied, the amount of cycles should decrease. More information surrounding this subject, is given in the next chapter.

The real values should be determined by experimental tests and be inserted afterwards in ANSYS to calculate the fatigue life and safety factor of the connection. However the estimated values are sufficient for the study of the vertical displacement.

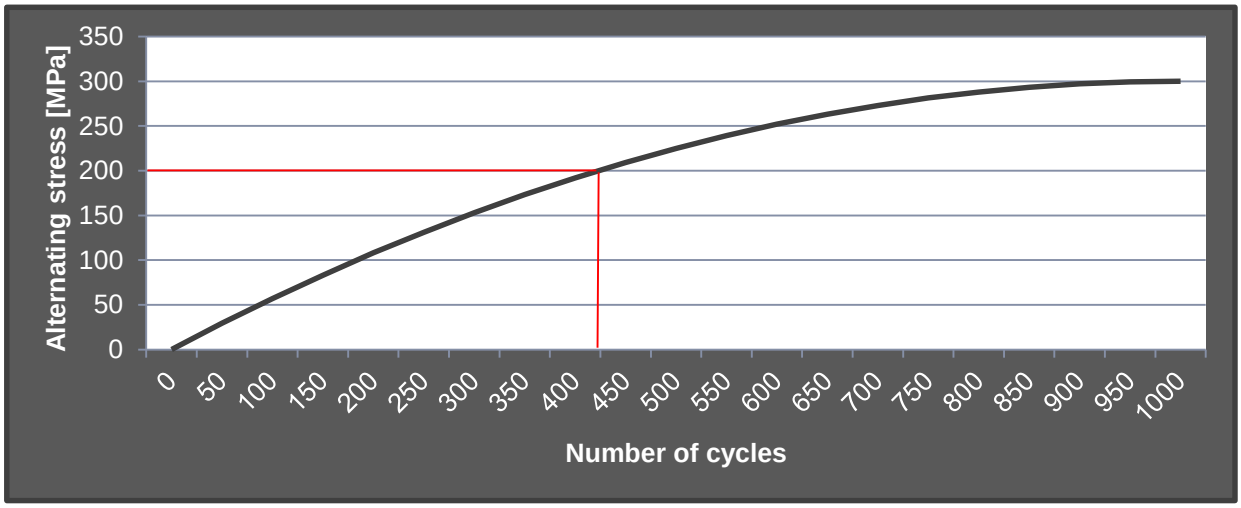

Figure 3.9 Alternating Stress Mean Stress curve

To subject a 3D-model to different loads and extract information such as deformations or stresses, it is necessary to define the mesh, Figure 3.11. A mesh is a collection of vertices, edges and faces that represent the shape of the 3D-model. Different shapes can be used to create a mesh, alter alia, triangles (2D), quadrilaterals (2D), tetrahedras (3D), pyramids (3D), prisms (3D), and hexaedres (3D). The mesh should be constructed as regular as possible to achieve better results. The smaller the mesh is designed, the more accurate the results will be. On the contrary, it will cost more time for the model to run and perform calculations if the mesh is designed small.

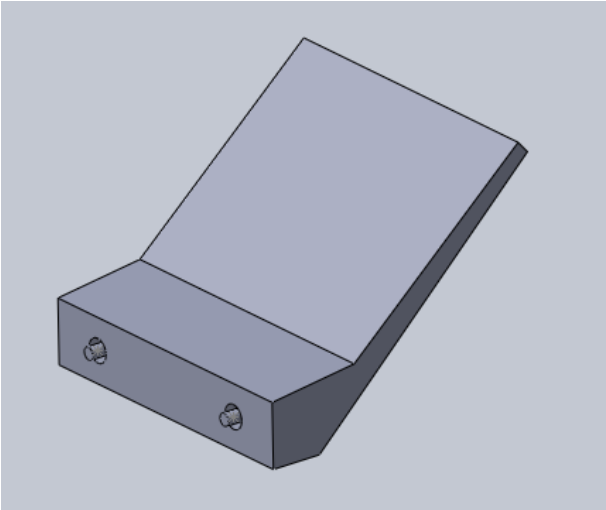

Figure 3.10 Construction in Solidworks

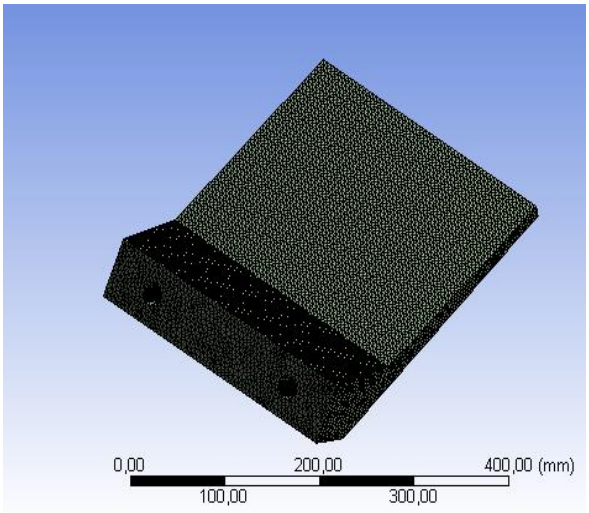

Figure 3.11 Mesh generation in Workbench

The two bolts are appointed to be the fixtures to the building. The next step is to apply the loads on the connection: Self-weight of the concrete, the effect of the wind on the opposite façade and frontal wind. The values for wind force has been determined in paragraph 3.2.1 and in Etudes de brises de soleil en beton fibre ultra haute performance (Llorens, 2015). In this particular case, the values from this latter study will be used. In reality, the slab has a length of 2,85m. The forces applied on half of the slab should be taken into account for one connection.

Actions can be classified in different categories :
.- Permanent actions *(G)*, which is in our case self-weight of the structure.
.- Variable actions *(Q)*, here known as wind force.
.- Accidental actions (A)
.- Prestressing (*P*)

Because of the different loads, combinations should be made for the Ultimate limit state and Serviceability limit state. (EN 1990: Eurocode 0: Basis of structural design, 2002) Ultimate limit states concern the safety of the and/or of the structure. Serviceability limit states concern the comfort of people, appearance of the construction works, the functioning of the structure or structural members under normal use.

Safety coefficients and combination coefficients for expression (3.29) in different situations can be found in Table 3.12. All parameters are included in the table, although snow is not relevant here. Combination of loads for the Ultimate limit state and Serviceability limit state:

$$\sum_{j\geq 1} \gamma_{G,j} * G_{k,j} + \gamma_p * P + \gamma_{Q,1} * Q_{k,1} + \sum_{i\geq 1} \gamma_{Q,i} * \psi_{0,i} * Q_{k,i} \qquad (3.29)$$

Table 3.12 Safety coefficients and combination coefficients

Combinations of actions			
Combination coefficients			
Action	Type	Combination coefficient	
Imposed loads on buildings	Combination value for variable action	$\psi_0 =$	0,7
	Frequent value for variable action	$\psi_1 =$	0,5
	Quasi–permanent value for variable action	$\psi_2 =$	0,3
Wind	Combination value for variable action	$\psi_0 =$	0,6
	Frequent value for variable action	$\psi_1 =$	0,2
	Quasi–permanent value for variable action	$\psi_2 =$	0,0
Snow (h< 1000m)	Combination value for variable action	$\psi_0 =$	0,5
	Frequent value for variable action	$\psi_1 =$	0,2
	Quasi–permanent value for variable action	$\psi_2 =$	0,0
Safety coefficients			
Ultimate limit states			
Permanent actions		$\gamma_G =$	1,35
Variable actions		$\gamma_Q =$	1,50
Serviceability limit states			
Permanent actions		$\gamma_G =$	1,00
Variable actions		$\gamma_Q =$	1,00

Wind cannot be applied on the structure in two different directions on the same time. This gives three usable combinations in the ultimate limit state:

$$1{,}35 * G_{k,j} \tag{3.30}$$

$$1{,}35 * G_{k,j} + 1{,}50 * Q_{k,1} \tag{3.31}$$

$$1{,}35 * G_{k,j} + 1{,}50 * Q_{k,2} \tag{3.32}$$

$G_{k,j}$ is automatically calculated by the program, based on the density and the standard earth gravity acceleration of 9806,6mm/s². The self-weight of the half of the slab should be taken into account. Therefore, an extra acceleration is added because ANSYS only calculates the self-weight of the piece inserted in the program (30cm). The wind forces determined in chapter 3.2.1 should be multiplied by a factor for the same reason. Factor: (2,85m/2)/0.30m = 4,75. Given for $Q_{k,1}$ = -7,0390E-4MPa, $Q_{k,2}$ = 2,21984E-3MPa, a value of 3,344E-3MPa and 1,0544E-2MPa respectively.

The vertical deformations are calculated with ANSYS for the ultimate limit state and the results of the combinations are shown in Figure 3.12, Figure 3.13 and Figure 3.14. Maximum deformations of the different combinations:
For expression (3.30)(3.20) **= 0,42186mm.**
For expression (3.31) = -0,57163mm.
For expression (3.32) = 3,5545mm.
The maximum value of vertical deformation will be used: 3,5545mm.

The frequency can be found by using Table 3.13 and depends on the type of structure (cladding). This indicates a value for the duration of the gust of three seconds or in other words, a period of three seconds.

$$f = 1/T \tag{3.33}$$

T is the period and f is the frequency. The necessary frequency is equal to 1/3Hz = 0,33Hz.

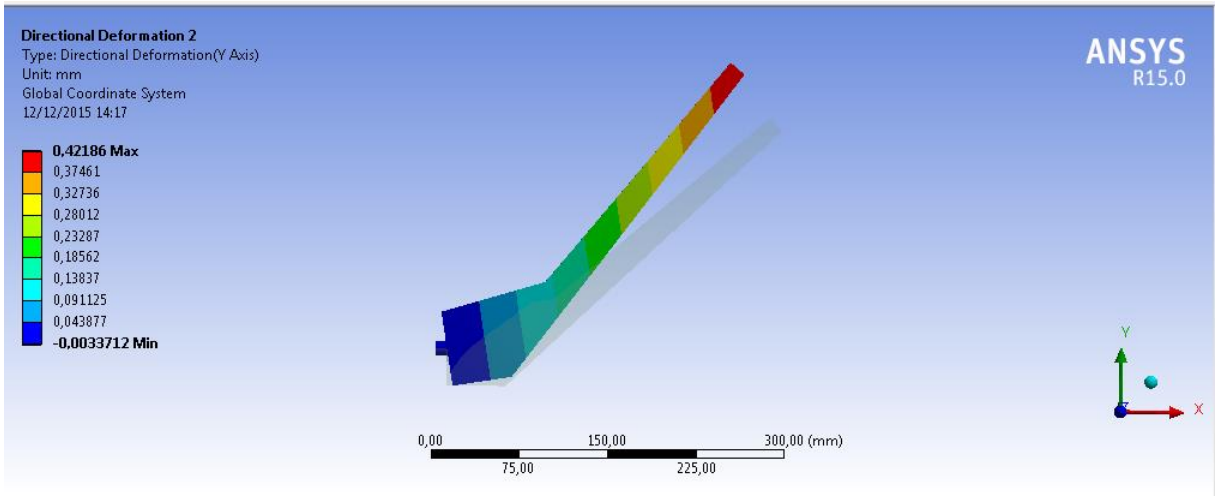

Figure 3.12 Vertical deformation, self-weight

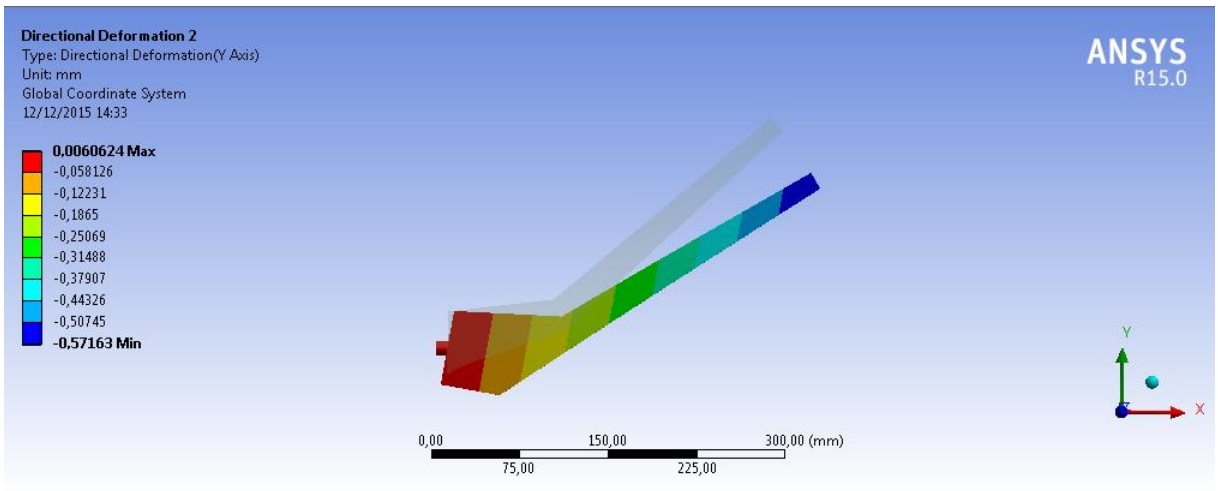

Figure 3.13 Vertical deformation under self-weight and wind on opposite façade

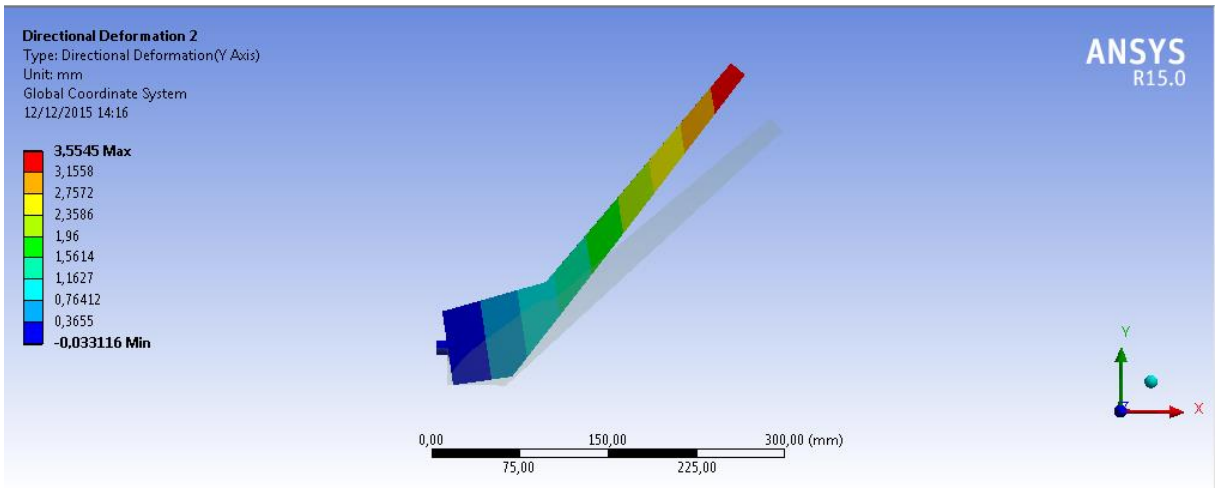

Figure 3.14 Vertical deformation under self-weight and wind on cladding

Table 3.13 Gust duration

Structural type	Duration of the gust
Elements and fixtures	
- Isolated structural elements - Substructures (e.g. cladding, roofing, etc.) and their attachments to the structure	3 seconds
- Structures or parts whose greatest horizontal and vertical dimension does not exceed 50m	5 seconds
- Structures or parts whose greatest horizontal and vertical dimension does exceed 50m	15 seconds
Elements and mobile facilities	
- Equipment - Equipment and facilities for transport of goods	3 seconds
-Small boats and floating elements with a length up to 25m	15 seconds
-Ships and floating elements with a length bigger than 25m	1 minute

3.3 Conclusion

Wind can be separated in static and dynamic components. Fatigue failure of structures and elements is induced by the cyclic dynamic components known as the wind gusts and turbulence. The characteristics for the simulation of a wind gust in Marseille are determined and joined in Figure 3.15.

Table 3.14 Test conditions

Test conditions	
Frequency	0,33Hz
Displacement	3,55mm
Threshold conditions	[0,4mm/sec ; 2mm/sec]

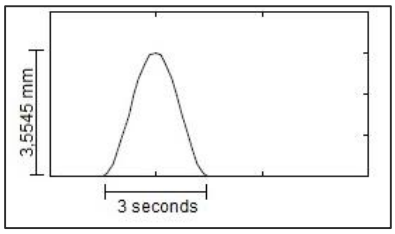

Figure 3.15 Simulation of 1 gust

The boundary conditions, shown in Table 3.14, are specified based on experience. Testing below a velocity 0,4mm/sec is too slow and above 2mm/sec is too fast.

4 Test in laboratory conditions

4.1 History of wind performance evaluation

The last three decades, wind induced failure gasped more attention because of the construction of higher and slimmer buildings. Tests and studies were conducted to simulate the wind effect. In the beginning, static test were applied on construction. Due to the investigation of premature failures, especially on roofcladdings, the knowledge has grown that wind should be evaluated with dynamic experiments. The well-known wind tunnel test is most used today.

4.1.1 FM 4470 and UL 580 standard

Figure 4.1 UL 580 , uplift test

Fatigue has been tested by many various procedures. In Canada, Baskaran and Dutt (1995) described and simulated wind on roofs as loads sequences in two different standard tests: The load sequence for the Factory of Mutual 4470 standard (FM 4470) and the load sequence for the Underwriters Laboratories 580 standard (UL 580), shown in Figure 4.1. The wind gusts are simulated by conducting pressure cycles for a certain timespan.

The FM 4470 load sequence is a test, designed to investigate the ability to resist to foot traffic on a roof. Later on, it was further developed to simulate wind. Initially it starts with a constant pressure of 1400Pa for one minute. Every minute, the pressure is increased by 700Pa until failure. It can be stated that this test applies static loading and therefore doesn't qualify to be used for fatigue testing. The test does not ask for a lot of time, one test can be finished in 10minutes.

The UL 580 test is designed to test uplift wind and starts as well with subjecting the roof to a constant pressure. However, the initial pressure is a negative pressure of 2330Pa and is applied for 5minutes. During the tests, positive and oscillating negative pressures are excited in different phases. The test area is a room from 10x10m.

Because of the lack of ability to simulate the realistic field conditions, these tests were evaluated as inadequate to test fatigue. In Europe, fatigue testing was already in a more advanced stage.

4.1.2 European and Norwegian load sequences

The UEAtc load cycle, Europa, by Gerhardt and Kramer (1986) was one of the first dynamic tests, containing time-varying loads applied on mechanical fixings. The wind forces are represented by different cycles of gusts, shown in Figure 4.2. The process contains four main steps:

- 4 x 1415 gusts with a maximum load of 300N
- 200 000 fluctuations (frequency: max 10Hz) with a load of 100 N
- 1415 gusts with a maximum load of 400N
- Increase with 100N every 1415 gusts until failure.

It takes one day to complete the test which is very time-consuming.

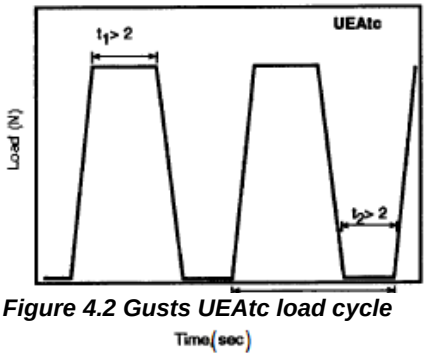

Figure 4.2 Gusts UEAtc load cycle

Another test procedure based on applying pressure on the tested specimen by simulating gusts, is the NBI 162-90 evaluation standard developed by the Norwegian Building Research Institute (1987). An upper and a lower box are installed with in the middle the specimen. A simulated wind is excited by a static pressure in the lower box and a pulsating suction in the lower box. The gusts have a length of 15 seconds for one hour, subsequently the pressure is increased every hour until failure.

4.1.3 Wind tunnel

In the 20th century, approximately in the thirties, fundamental development for the current techniques for wind tunnels was done in Gottingen in Germany. The wind tunnels were used to do tests for aerospace engineering. The experiments were conducted in flows with a low turbulence. The basic principles for wind tunnel study today were determined at that time.

To this present day, wind tunnel testing became one of the most common methods to simulate wind. Because of the limited dimensions of a wind tunnel, a scale model of the building and surroundings should be created. The wind velocity and wind gusts should be increased or reduced according to the scale. Guidelines for this scaling and the use of the wind tunnels were made by ASCE, WTG and BLTWL.

Inside the tunnel, the wind velocity, forces, pressure, accelerations and moments can be measured. The used data is mostly transferred into non-dimensional coefficients for studies about wind loads. In the next paragraph, wind forces will be determined based on non-dimensional pressure coefficients. Wind is excited in long tunnels by ventilators to create a natural environment. Other elements such as devices to control the flow coming from the fans, an adjustable working section, an outlet for the flow, etc. can be found inside the wind tunnel to simulate realistic conditions. The types of tunnels can be distinguished: open and closed section tunnels. In this latter, the wind flow is recirculated through ducts.

4.2 Fatigue

4.2.1 S-N curve

A material gradually deteriorates when subjected to cyclic loads. Fatigue life is separated in three different stages: crack initiation, crack growth and finally, rapid rupture. The amount of necessary cycles (N) at a varying constant amplitude stress (S) to cause rupture is shown in Figure 4.3. Fatigue life is commonly plotted in an S-N diagram and can be defined as the total number of stress cycles required until failure occurs.

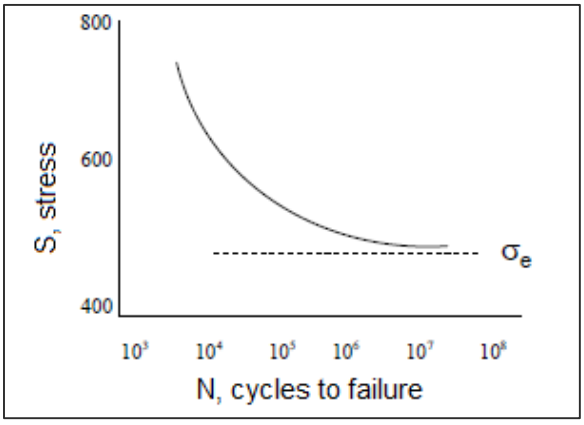

Figure 4.3 Stress-life curve

For some materials, an endurance limit, σ_e, can be found. Below this stress, the material will not fail due to fatigue. In other words, the amount of cycles can be infinite below the endurance limit. Other materials do not exhibit such a behaviour. Fatigue life is not a fixed property of a material but can be influenced by a lot of parameters such as surface finish, size, temperature, stress concentration, etc. The scale of the number of alternating stress cycles is a logarithmic scale because the necessary amount of can rapidly increase to 10 000 or 100000 cycles.

4.2.2 Cyclic stress

A cyclic stress is determined by its mean stress, alternating stress, maximum stress and minimum stress. The mean stress, σ_{mean}, is the value exactly in the middle of the maximum stress and the minimum stress of one cycle. The alternating stress, $\sigma_{alternating}$, is the difference between the peak stresses and the mean stress, this is the so called stress amplitude:

$$\sigma_{mean} = \frac{\sigma_{max} + \sigma_{min}}{2} \quad and \quad \sigma_{alternating} = \frac{\sigma_{max} - \sigma_{min}}{2} \tag{4.1}$$

The stress ratio, R, and the amplitude ratio, A, depend on these four stresses:

$$R = \frac{\sigma_{min}}{\sigma_{max}} \quad and \quad A = \frac{\sigma_{alterning}}{\sigma_{mean}} \tag{4.2}$$

Based on the stress ratio and amplitude ratio, a loading cycle can be called fully reversed (R = -1 and $A = \infty$), zero reversed (R = 0 and $A = 1$), or fluctuating (R= value and A= value). These three types are shown in Figure 4.4, Figure 4.5 and Figure 4.6.

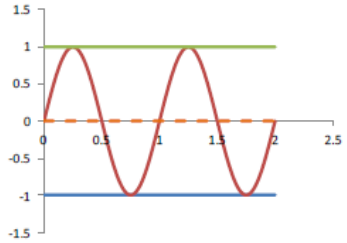

Figure 4.4 Fully reversed

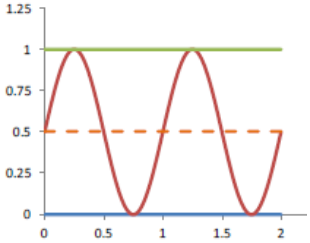

Figure 4.5 Zero reversed

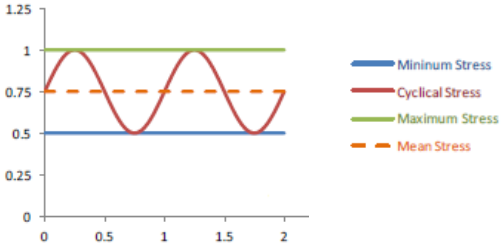

Figure 4.6 Fluctuating

4.3 Design of the setup and procedure

To test the fatigue resistance of the bolted connections, a hydraulic fatigue testing machine is used, namely the Servosis ME 402E. This machine has the ability to test tensile strength, compression strength and fatigue life of a material. Two different tests can be performed to determine fatigue life with this apparatus. For the first one, a load is applied on the test piece with a certain frequency. The induced displacement will be measured. Based on the changes in displacement, fatigue life can be calculated. The second approach is the approach used in the following tests. A vertical displacement will be given to the test piece while the force needed to obtain this displacement is measured. The necessary parameters are determined in chapter 3 and could be found in section 3.3.

4.3.1 First approach

First, the connection of the test specimen of 30cm was secured to the base of the apparatus (Figure 4.7). Followed by drilling four holes in the slab (Figure 4.8) to secure a metal plate on it (Figure 4.9). This plate is used to transfer the loads from the apparatus on the slab to excite the vertical displacement. The next step is to adjust the parameters (Figure 4.11). The frequency is a constant value. The amount of cycles and the amplitude changes for three different phases. These variables are based on a fatigue loading sequence designed for hurricanes according to the Florida Building Code. In our case, p is the amplitude. The connection is tested to resist this fatigue load sequence.

Figure 4.7 Tested connection

Figure 4.8 Drilled holes

Figure 4.9 Metal plate

Figure 4.10 Loads directly on slab

Figure 4.11 Set-up of the test conditions

Table 4.1 Fatigue loading sequence

Range of test	Number of Cycles
0 to 1,0p	600
0 to 0,6p	70
0 to 1,3p	1

4.3.2 Conclusion of first approach

The first test with this procedure failed, due to a space between the metal plate and the slab. The second test was performed by applying the loads directly on the slab (Figure 4.10). Hence, the metal plate was removed and the test was performed once more. It did not lead to failure of the connection.

4.3.3 Second approach

The second approach entails applying loads on the test specimen to generate the same displacement for every cycle until failure occurs. The program, used in previous procedure, is unable to output only the maximum forces. Therefore a load cell, shown in Figure 4.12 and Figure 4.13, is used which makes it able to register the force every 0,5 seconds. The results of this test, are discussed in the following paragraph.

Figure 4.12 Attaching load cell

Figure 4.13 Test with load cell

4.4 Experimental results

The parameters of the previous approach were used. This means an amplitude of 3,55mm and a frequency of 0.34Hz. The difference in this approach is that the amount of cycles is not predefined. The first 500 cycles are represented in Figure 4.14 and indicate that the initial force needs a certain amount of cycles to stabilise. The x-axis is the displacement, it variates between circa 20mm and 23,5mm. The y-axis is the force needed to obtain this displacement. Figure 4.15 Shows a stable loop of forces after 1500 cycles.

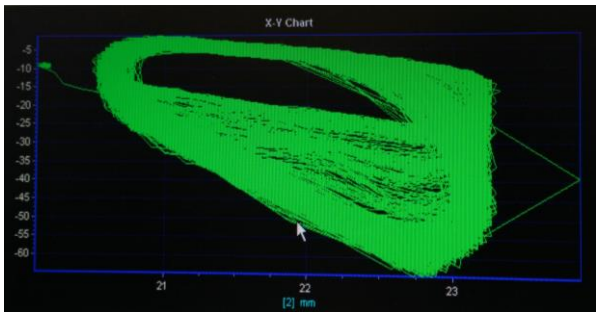

Figure 4.14 First 500 cycles (A = 3,5545mm)

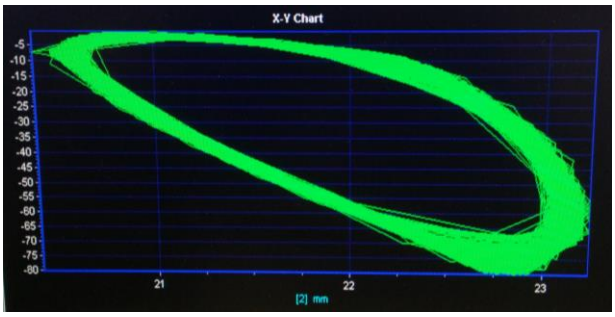

Figure 4.15 After 1500 cycles (A= 3,5545mm)

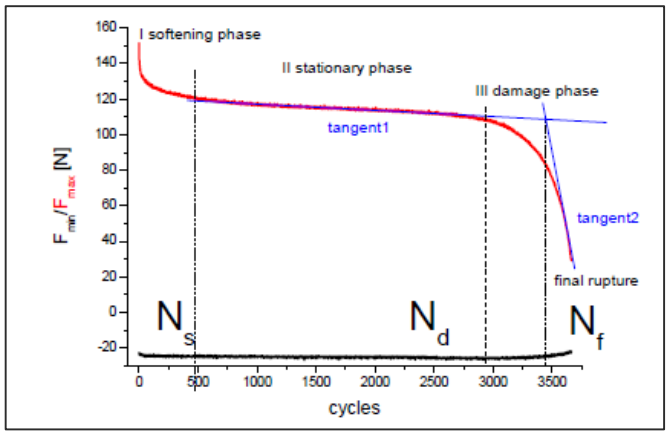

Figure 4.16 Example Fmax-cycles graphic (Major, 2012)

The purpose is to compose a graphic were the different phases of fatigue can be shown based on the maximum required force. (Major, 2012) An example of such a graphic is shown in Figure 4.16. A high force should initially be required and should decrease rapidly in the softening phase (crack initiation), followed by a stationary phase (crack growth) until the damage phase (final rupture). Figure 4.17 shows that the tested specimen behaves differently. The specimen requires approx. 750 cycles to obtain a constant maximum force. Hereafter it arrives at the stationary phase.

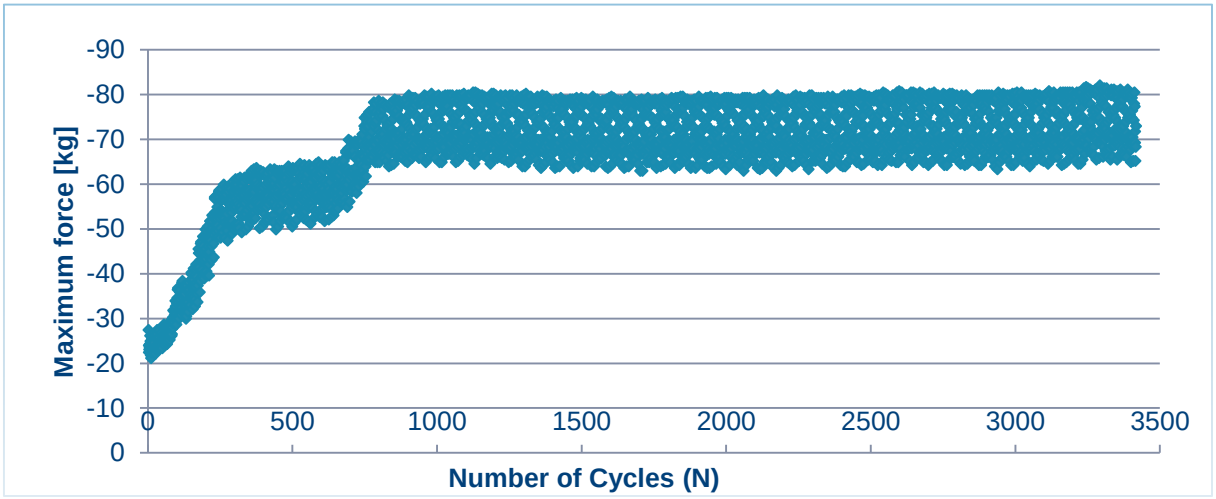

Figure 4.17 Fmax - number of cycles (A= 3.5545mm)

After applying 3500 cycles, no variation in forces appeared. Therefore the procedure was changed. At first a bigger displacement, 6,3mm, was applied on the same construction for 700 cycles. Next, the amplitude was increased to 9mm for 200 cycles and at last a maximum displacement of 12mm was used for again 200 cycles. The frequency remained the same. The required maximum forces according to the number of cycles are shown in Figure 4.18.

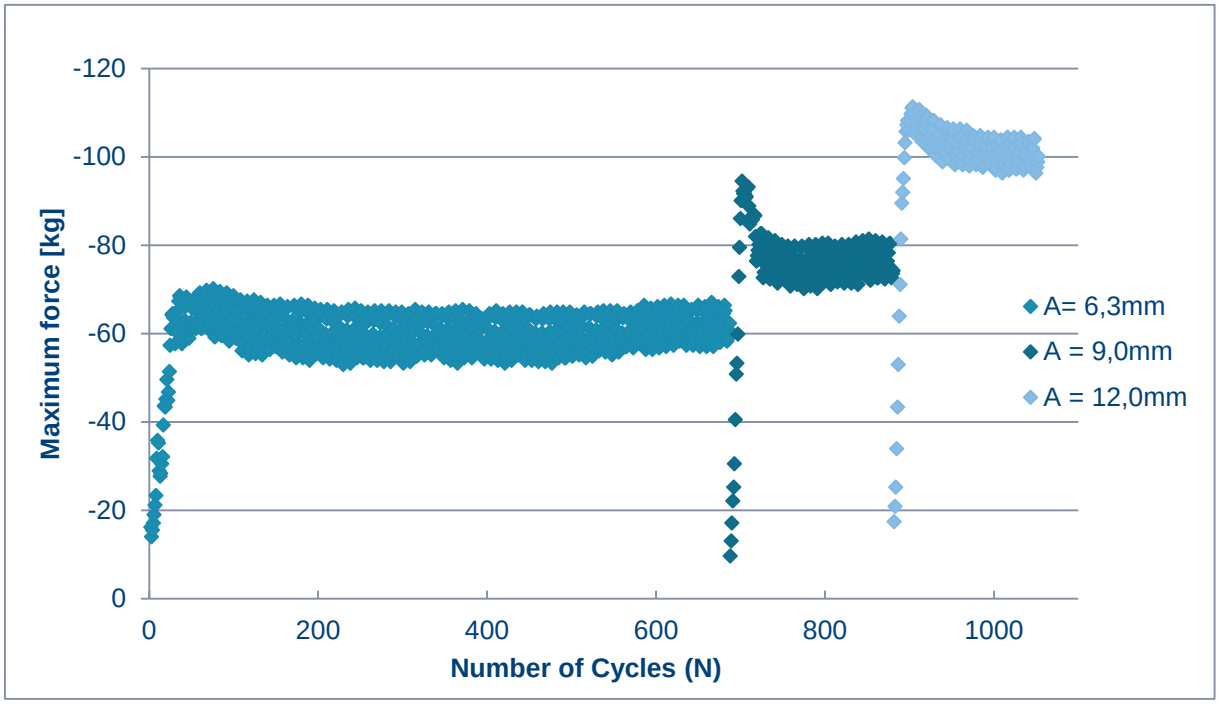

Figure 4.18 Fmax-Cycles (A = 6,3mm; A = 9mm; A = 12 mm)

It was unexpected that the maximum force would be lower for a displacement of 6,3mm than for a vertical deformation of 3,55mm. This phenomenon can be explained when comparing Figure 4.19 with Figure 4.20 and Figure 4.21. The metal plate bends which indicates that it suffers more under a bigger amplitude than the slab. Before performing the tests, the focus was on the connection of the bolts and the concrete slab. The fact that the metal plate deforms points out that not only the connection should be carefully studied but the secondary structure as well.

Figure 4.19 A=3,55mm

Figure 4.20 A = 6,3mm

Figure 4.21 A =12mm

The slab was unscrewed after applying 200 cycles at an amplitude of 12mm to evaluate the bolts, Figure 4.22, and the socket, Figure 4.23. Observation: the bolts and the socket did not deform.

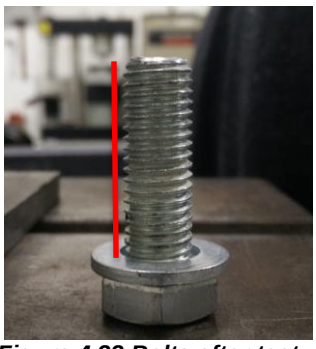

Figure 4.22 Bolts after test

Figure 4.23 Connection after test

4.5 Conclusion

The metal plate deforms and the bolts did not bend after applying the cyclic loads. Therefore the assumption can be made that the weakest part of the system could be the welds of the secondary structure.

The behaviour of the connection does not only depend on the connection between concrete and bolts. The joint to the secondary structure should also be taken into account to improve the behaviour of the system. A consequence of this is that more attention should be paid to welds.

Avoid contact between the concrete and the steel. When the test was performed with a bigger deformation, the concrete slab rotated in such a manner that the distance between the top edge of the slab and the metal plate increased and the bottom edge was pressed against the plate. The UHPFRC crumbled where it touched the metal plate.

Since the deformation is partly absorbed by the steel plate, the entire system must be studied. The steel profile of the secondary structure was fixed on the workbench for this test. This profile is much longer in reality and will experience a bigger displacement.

5 Theoretical approach

5.1 ANSYS procedure

The following sections are a description surrounding the calculation of fatigue life in ANSYS. The beginning of this procedure is already described in section 3.2.2 (Gusts).

5.1.1 Fatigue tool

The procedure resumes after defining the mesh. From there on the fatigue analysis should be chosen to determine the safety factor and fatigue life by inserting a fatigue tool. The fatigue tool entails the constant amplitude load and the different mean stress correcting theories that can be used.

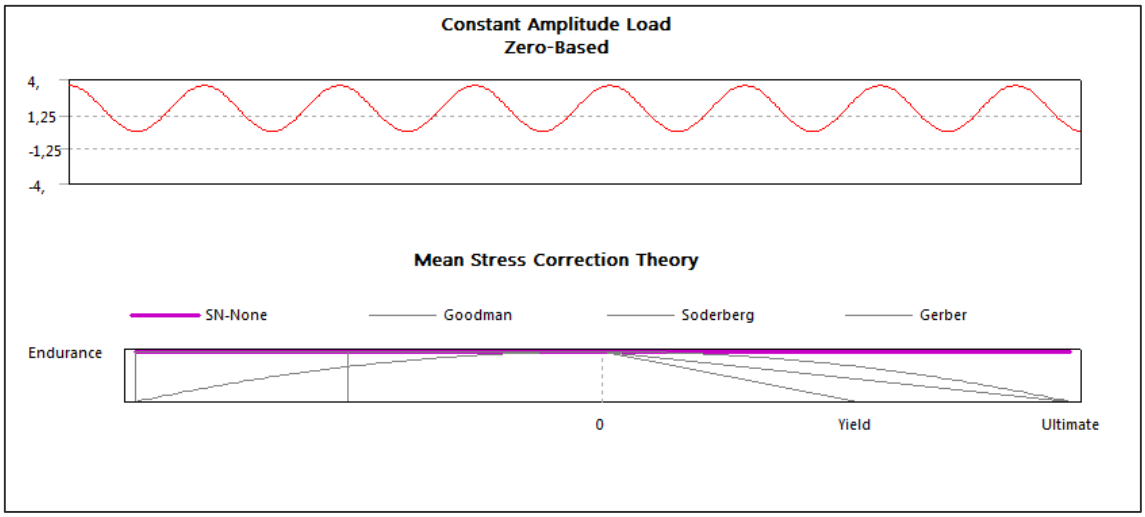

Figure 5.1 Fatigue tool screenshot

The constant amplitude load is discussed in paragraph 4.2.2 and is shown in Figure 4.4, Figure 4.5 and Figure 4.6. The four different options are: fully-reversed, zero-reversed, fluctuating (in ANSYS is this called ratio) or historical data could be inserted. To simulate the experimental test as much as possible, zero-reversed should be selected.

For the mean stress correction theory, the choice should be made between the Goodman, the Soderberg, the S-N or the Gerber fatigue life stress theory. S-N represent the default theory. These empirical methods determine different curves to link the endurance limit on the alternating stress axis, (vertical axis) to either ultimate stress, σ_u, the yield stress, σ_y or the true fracture stress σ_f on the mean stress axis (horizontal axis). Empirical curves to estimate mean stress effects on fatigue life are shown in Figure 5.2.

General remarks: These methods should be used for tensile mean stress values only. Mostly used or accepted are the Goodman and Gerber curve. The Goodman approach is the simplest method and therefore the least accurate but in general there is little difference for all methods when the stress ratio is small. If the stress ratio approaches 1, a large difference is shown in the models. The Soderberg method is only valid when fatigue failure of yielding does not occur.

Taking all this information into account, the Goodman theory is assumed to be best suitable in this particular case with as stress component the Von Mises stress.

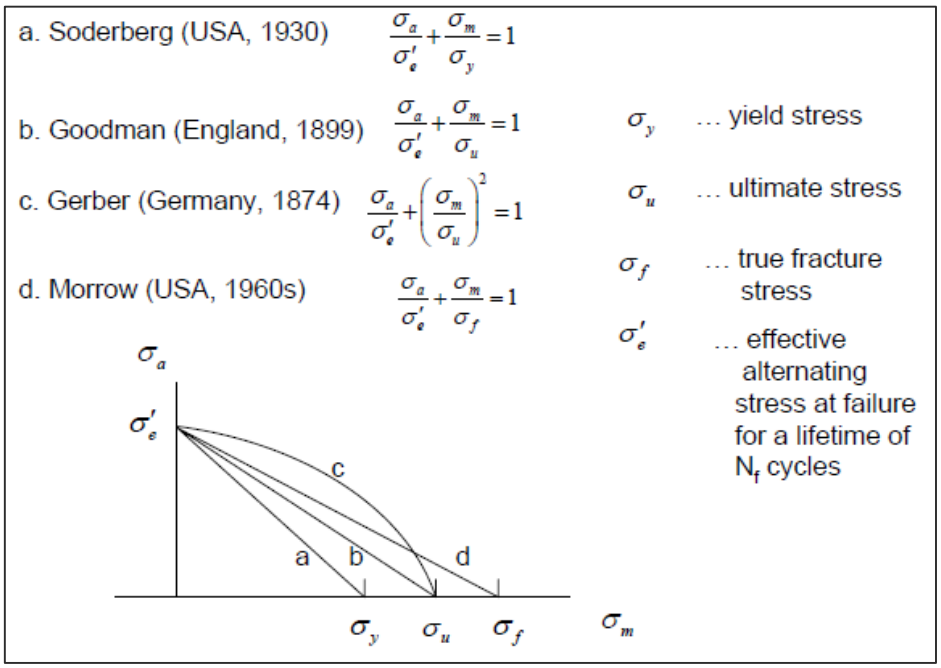

Figure 5.2 Graphical comparison empirical curves (Fatigue Life evaluation, 2011)

5.1.2 Further process

After inserting the parameters in the fatigue tool, the loads should be applied and the bolts should be appointed as the fixtures (paragraph 3.2.2). A last adjustment should be made: the realistic fatigue life curve of the concrete should be inserted in the Engineering data-window. The next step is to let the program solve this case and generate fatigue life and the safety factor. The safety factor variates according to the chosen mean stress correction theory.

5.2 Conclusion

It was not possible to compare the results of the experimental test with those from the calculations due to the inconclusiveness of the experimental tests. Instead the procedure to generate the safety factor and fatigue life is given.

6 Further research

The aim was to design a procedure to calculate fatigue life. More tests should be performed at different amplitudes to construct an S-N life cycle. If more tests are performed, the possibility arises to compare the results with the numerical model constructed in ANSYS. The final experimental procedure in this study was only performed once. The tests should be repeated on least five elements with the same constant amplitude during all the tests to verify the result.

Noticing the complexity of the situation, it would be recommended to split the set of test in different components. Not only the connections with the bolts and the concrete should be designed in ANSYS and experimentally tested but also the entire system. This gives the following options:
.- Study the behaviour of the complete system.
.- Perform different fatigue tests for the individual components: Bolts, connection between concrete and bolt, concrete, metal plate, secondary structure and connection with the secondary structure.

General conclusion

The use of ultra-high performance fibre-reinforced concrete for structures is rapidly gaining more popularity due to the important improvements of properties. Slimmer structures or elements can be designed because of the improved characteristics of this kind of concrete. This creates a lot of new opportunities in terms of structural and architectural design. Within the scope of this report, thin concrete slabs with a length of 2,85 meter were used.

For the purpose described in this thesis, the fixing socket with bolt is stated to be the most adequate for the bolted connections. These latter can fail due to two types of loads: static loads or dynamic loads. The static tests were already carried out to investigate the actual tensile strength and the bonding of the socket with the concrete. The behaviour if the connection subjected to cyclic loads on a long-term basis remained undetermined. Hence, an experimental test was designed to investigate the fatigue life of the connection.

A procedure was designed to apply cyclic wind loads on the test specimen by using a servo-hydraulic fatigue testing machine. Before the test was conducted, some key parameters were determined such as the frequency and the amplitude of a wind gust, the wind forces and the wind velocity. The assumptions necessary for the calculations were based on the site of Marseille.

The tests resulted in the deformation of the metal plate. This plate connects in reality the bolts and the concrete slab to a steel profile on the building. The bolts, the bonding to the concrete and the concrete itself did not receive any noticeably negative influences of the cyclic loads. The main conclusion of the tests was that the welds of the metal plate to the steel profile would probably be the weakest component of the connection. Further research should include studies about the various components of the connection and the different combinations of these elements.

Unfortunately, the tests did not result in a comparable value with a numerical model. A test with a longer duration and only one set of parameters should be excited to obtain such a value. To verify the result, the same experiment should be repeated several times.

References

(n.d.). Retrieved from leviaducdemillau: http://www.leviaducdemillau.com/en_index.php

Prof. S.R.Satish Kumar and Prof. A.R.Santha Kumar . (n.d.). *Design of Steel Structures.*

A. Baskaran et al. . (1999). A new facility for dynamic wind performance evulation of rooging systems. *Proceedings of the Fourth international Symposium of Roofing Technology* (pp. 168-178). Ottowa, Ontario, Canada: National Research Council Canada.

ACI Committee 544. (1993). *Guide for Specifying, Proportioning, Mixing, Placing, and Finishing Steel Fiber Reinforced Concrete.* American Concrete Instutite.

Amaya, G., Cooz, U., Gonzalez-Longatt, F., & Duran, M. (2012). *Modelado del Viento para Simulaciones Computarizadas de Sistemas de Potencia.*

Anchor systems. (n.d.). Retrieved from Hilti: https://www.us.hilti.com

Azeez, A. A. (2013). *Fatigue Failure and testing methods.* Riihimäki, Finland: HAMK.

Baskaran et al. (1997). *Wind performance evaluation procedures for roofing systems current status and future trends.* Canada: National research council.

Batoz, J.-F. (2009). *UHPFRC development on the last two decades: an overview.* Marseille, France: AFGC.

Behloul, M., Lee, K.C. (2003). *Ductal Seonyu footbridge, Journal 'Structural Concrete' , Vol 4, No 4, pp 195-201.*

CAE Nederland B.V. (2005, Februari 24). *Folley sanatorium Zonnestraal Hiversum*. Retrieved from Ultra hoge sterkte beton, Al het laatste nieuws en informatie over (vv)UHSB: http://www.uhsb.nl/?p=150

Department of transportation, State of California. (2012). *Bridge Design Aids 5-81: Anchorage to Concrete.* Sacramento.

EN 1990: Eurocode 0: Basis of structural design. (2002). Brussel: Bureau voor normalisatie.

EN 1991-1-4: Eurocode 1: Actions on structures - Part 1-4: General Actions - wind actions. (2005). Brussel: Bureau voor Normalisatie.

European Organisation for Technical Approvals. (2013). *ETAG 001 Guideline for european technical approval of metal anchors for use in concrete. Part one: anchors in general.* Brussels: EOTA.

Fastener Types. (2015). Retrieved from Concrete network: http://www.concretenetwork.com/concrete/concrete_fasteners/chemical_fasteners.htm

Fatigue Life evaluation. (2011). Retrieved from Iowa State university: http://www.public.iastate.edu/~e_m.424/Fatigue.pdf

Francois Toutlemonde and Jacques Resplendido. (2011). *Designing and Building with UHPFRC, State-of-the-Art and Development.* Great Britain and The Unites States: ISTE Lttd and John Wiley and Sons, Inc.

Gedeon, M. (2014, March). *Mean Stress and Alternating Stress.* Mayfield Heights: Materion Brush Inc.

Geurts, C. (n.d.). *The use of Wind tunnel experiments for wind loads on structures.* Delft, The Netherlands: TNO Built Environment and Geosciences.

Graybeal, Henry G. Russell and Benjamin A. (2013). *Ultra-High Performance Concrete: A State-Of-The-Art Report for The Bridge Community.*

HB anchor bolt systems. (n.d.). Retrieved from HALFEN: http://www.halfen.com/

Johnson, G. (2001). Chapter 2: Wind characteristics. In G. Johnson, *Wind energy Systems* (pp. 2.1 - 2.65). Manhatten: Kansas State university.

Kodama, A. O. (2009, March). Haneda Airport (Tokyo): Blurring the borders between sea and sky.

Llorens, M. (2015, October 6). Étude de brises soleil en beton fibre ultra haute performance. Girona, Gerona, Spain.

Major, Z. (2012). *Applicability of Displacement Controlled Fatigue Test Methods for Compliant Structures.* Brasov, Romania: IMEKO TC15.

Ocel, J., & Graybeal, B. (2007). *Fatigue behaviour of an ultra-high performance concrete I-girder.* McLean, Virginia: FHWA Turner-Fairbank Highway Research Center.

Parte 3 cargas de viento. (n.d.). Retrieved from ABC puertos: http://www.abcpuertos.cl/documentos/Rom_04/rom_04_95_3_Cargas_del_viento.pdf

Petr Maca, J. Z. (2010). *Development of Ultra High Performance Fiber Reinforced Concrete Mixture.* Prague, Czech Republic: IEEE Symposium of Business, Engineering and Industrial Applications.

PFEIFER Thread system the original. (2014, 10). Retrieved from PFEIFER: http://www.pfeifer.de/

Royance, D. (2001). *Fatigue.* Cambridge: Massechusetts Institute of Technology.

Statistiique de vent et meteo. (2015). Retrieved from Windfinder: http://fr.windfinder.com/windstatistics/marseille

Tieleman, H. (2003). Wind tunnel simulation of wind loading on low-rise structures: a review. In *Journal of Wind Engineering and Industrial Aerodynamics* (pp. 1627-1649). USA: Elsevier.

Villarrubia, M. (2015, Januari 12). *Energía eólica: Características de los vientos y su potencial*. Retrieved from Blog sobre: Tipos de Energia: http://tipos-de-energia.blogspot.com.es/2006/02/energa-elica-caractersticas-de-los.html

Wind scales. (n.d.). Retrieved from MarineWaypoints.com: http://www.marinewaypoints.com/marine/wind.shtml